Emergent complex quantum networks in continuous-variables non-Gaussian states

Mattia Walschaers, ^{1,*} Nicolas Treps, ¹ Bhuvanesh Sundar, ² Lincoln D. Carr, ³ and Valentina Parigi^{1,†}

¹ Laboratoire Kastler Brossel, Sorbonne Université, CNRS, ENS-Université PSL,

Collège de France, ⁴ place Jussieu, F-75252 Paris, France

² Institute for Quantum Optics and Quantum Information of the Austrian Academy of Sciences, Innsbruck A 6020, Austria

³ Department of Physics, Colorado School of Mines, Golden, Colorado 80401, USA

(Dated: July 28, 2021)

Large multipartite quantum systems tend to rapidly reach extraordinary levels of complexity as their number of constituents and entanglement links grow. Here we use complex network theory to study a class of continuous variable quantum states that present both multipartite entanglement and non-Gaussian statistics. In particular, the states are built from an initial imprinted cluster state created via Gaussian entangling operations according to a complex network structure. To go beyond states that can be easily simulated via classical computers we engender non-Gaussian statistics via multiple photon subtraction operations. We then use typical networks measures, the degree and clustering, to characterize the emergent complex network of photon-number correlations after photon subtractions. We show that, in contrast to regular clusters, in the case of imprinted complex network structures the emergent correlations are strongly affected by photon subtraction. On the one hand, we unveil that photon subtraction universally increases the average photon-number correlations, regardless of the imprinted network structure. On the other hand, we show that the shape of the distributions in the emergent networks after subtraction is greatly influenced by the structure of the imprinted network, as witnessed by their higher-moments. Thus for the field of network theory, we introduce a new class of networks to study. At the same time for the field of continuous variable quantum states, this work presents a new set of practical tools to benchmark systems of increasing complexity.

I. INTRODUCTION

Large multiparty quantum systems are extremely hard to describe, although the complex behavior of their quantum states is what makes them appealing resources for quantum information processing. Intensive efforts have been dedicated to the direct representation of quantum states via numerical and analytical approaches with the aim of classifying and detecting truly non-classical and useful quantum features, like entanglement[1, 2]. For example, tensor networks have been demonstrated to be very powerful tools for entanglement classification, and have been applied in many fields ranging from condensed matter physics to conformal field theory [3]. In the quantum information scenario, resource theories offer a general theoretical framework to classify useful resources to reach desired quantum features [4]. Different strategies that are becoming more and more popular exploit machine learning procedures [5, 6] to classify general complex features in the quantum realm [7–9] often by representing them via neural networks [10].

In this work we focus on the complex behaviour of quantum states in continuous variable (CV) quantum systems and we tackle it via complex networks theory. Our work is motivated by all-optical platforms, based on continuous quantum observables, that can already produce large entangled networks [11–13]. These networks are made of travelling light fields with quantum corre-

lations between amplitude and phase values of different modes of the field, e.g. light at different colors. They have Gaussian measurement statistics for amplitude and phase continuous variables, so that they can be easily simulated via classical computer. They are essential resources for measurement based quantum computing but, in order to perform quantum protocols, they must acquire non-Gaussian statistics of the continuous variables. Non-Gaussian statistics can be induced via mode-selective addition and subtraction of photons [14, 15], that are then called non-Gaussian operations. When the number of entangled systems – in our case optical modes – and the number of non-Gaussian operations are large enough, these systems are hard to benchmark [16–21] and computationally hard to sample [22].

We consider in this context network models studied in network theory to reproduce the features of real-world networks. The optical CV entangled networks can in fact be easily reconfigured in arbitrary shape [23]. They thus provide an excellent playground to explore whether mimicking real-world complex network structures [24, 25] provides an advantage for quantum information technologies, including quantum simulation and communication [23, 26] in a future quantum internet. Moreover, and this is a central point of our work, network theory gives us powerful tools for benchmarking these networks when affected by non-Gaussian operations. The used benchmark is based on calculation of photon-number correlations, a problem that for these systems in the most general case belongs to the #P complexity class (see A 3). We restrict our analysis to a less complex but tractable case, that allows for collecting and processing significant statistics

^{*} mattia.walschaers@lkb.upmc.fr

[†] valentina.parigi@lkb.upmc.fr

via complex network techniques. We can then study how different network shapes can support, enhance, spread or destroy the non-Gaussian features provided by these local operations.

A. Complex networks and quantum physics

In the last decades, network theory has made significant progress in describing collective features and functionality of complex systems [27, 28]. Network-based descriptions are pivotal in social and biological science as well as in technological infrastructures like power grids and information networks such as the internet. The study of complex network structures has spread in physics [29, 30] helping in the description of complex physical systems. Subfields in physics utilizing complex networks include statistical physics, condensed matter and quantum physics with, e.g., the study of the Ising model and Bose Einstein condensation [31–37]. More recently the study of complex networks has become relevant for quantum systems and procedures employed in quantum information technologies [24, 25, 38–42] indicating that a dedicated theory of quantum complex networks needs to be built, especially for networks with no classical equivalent, like those based on quantum correlations or quantum mutual information. In particular, emergent complex networks based on quantum mutual information have determined critical points for quantum phase transitions [36, 43, 44]. Likewise, complex network theory has been successful in determining self-similarity in entanglement structure of spin-chains [45] as well as new kinds of structured entanglement emerging from quantum cellular automata [46] on qubit/gate/ciruit-based quantum computers. Networks are naturally evoked in the quantum regime in relation to the quantum internet [47], where it is not clear yet if the best arrangement of its components will take a complex shape as the classical internet. Networks are however pivotal in all quantum technologies. Indeed, quantum information algorithms and quantum transport can be mapped on quantum walks on regular and complex networks [48–51]. Complex networks also describe networked noisy intermediate-scale quantum computers [52, 53], imposing a crucial role for networks in near-term quantum information processing. Thus complex network theory provides a versatile toolbox, as it can be applied on different quantum features, and is very efficient in revealing emerging collective structural mechanisms.

Here we apply, for the first time, complex network analysis to CV multipartite quantum states. We focus on the ones that can be generated in the more advanced optical platforms, but the used methods can be applied on general CV states.

B. Conceptual scheme

The conceptual scheme of our analysis is shown in Fig. 1. Large CV entangled networks have been deterministically implemented via non-linear $\chi^{(2)}$ optical This operation entangles different modes processes. (be they spatial, spectral or temporal) of the fields via an appropriately engineered parametric interaction [11– 13, 23, 54, 55]. These processes are sketched in the left corner of the upper row of Fig. 1, where the different modes are represented by different colors. The circuit representation of the generated states is sketched in the second row of the figure: the non-linear optical process is equivalent to different travelling optical modes occupied by squeezed vacuum states that are entangled via C_Z gates. This generates the cluster state [56, 57]. In the third row we show the graphical representation of the state: the different optical modes are represented by different nodes of the network which are linked by C_Z gate entangling operations, counted by the entry 1 in the adjacency matrix A of the network. This structure is an *imprinted* network, as it builds the initial quantum states. In the right side of the first column of Fig. 1 we picture the action of multiple-photon subtraction, i.e. the repeated application of the photon annihilation operator \hat{a} on one specific mode of the field. The probabilistic implementation of this operation consists of a mode-selective beam-splitter that sends a small fraction of light to a photon counter: when n photons are detected an n-photon-subtracted state is heralded. The process can be implemented via non-linear interaction with supplementary gate fields [14]. In the fourth row of the first column we show the network of photon-number correlations between the different field modes that emerge from the imprinted network. This is the *emergent* network. Its adjacency matrix \mathbb{A} contains continuous values between 0 and 1, indicating the strength of photon-number correlations between couple of nodes. In this work we are interested in following the changes of this emergent network of photon number correlations after photon-subtractions on one node as a benchmark of the desired non-Gaussian properties of CV quantum states.

The role of complex networks in this work will be twofold. First, we consider complex network structures for the *imprinted* network of entangling C_Z gates, as shown in the third row of second column of Fig. 1. We will use complex network models that reproduce particular features of real-world networks. Second, we probe the impact of photon subtraction on the emergent networks by analyzing typical network measures, like degree and clustering, that quantify number of links and their structure and that are mostly used to characterize complex networks.

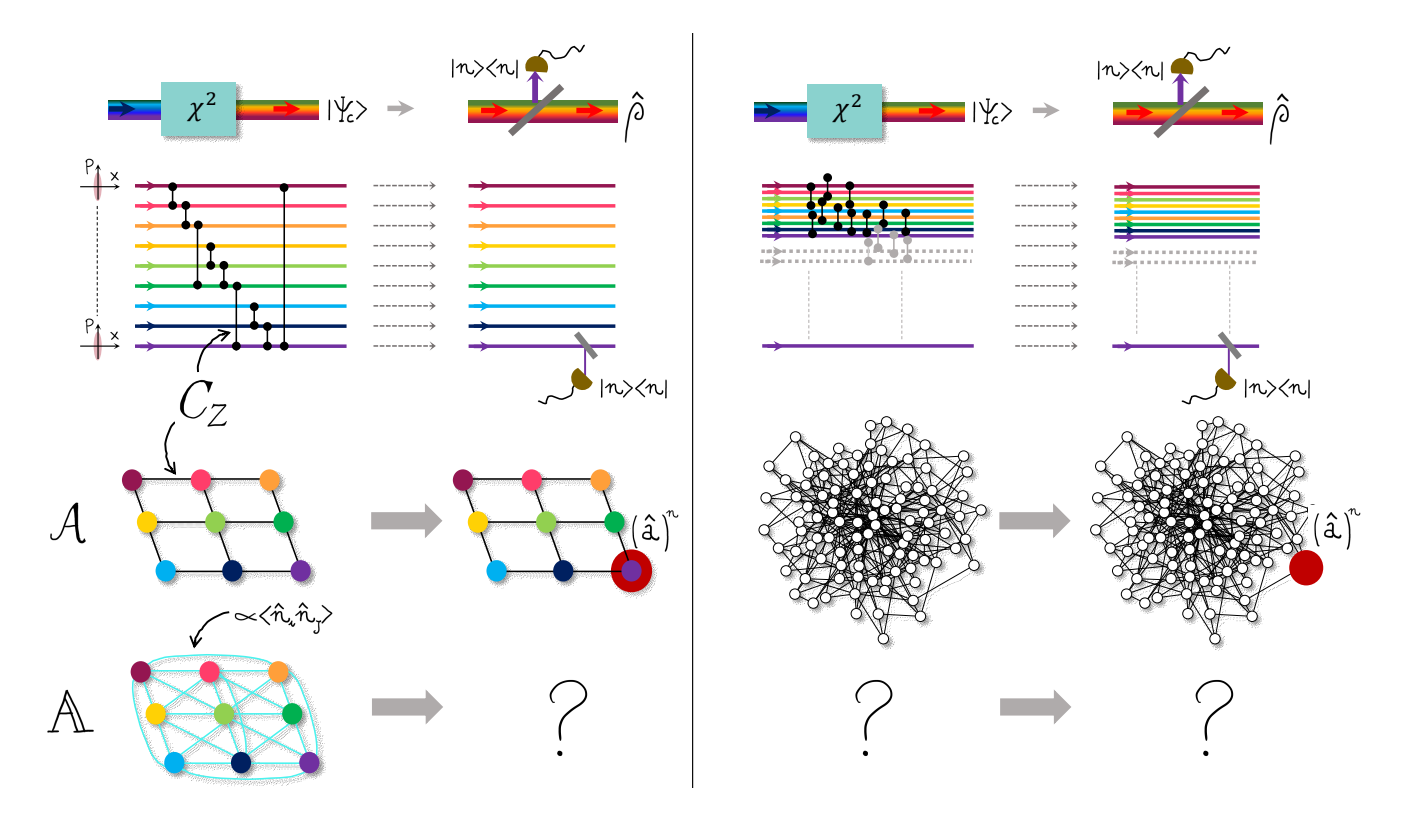


FIG. 1. Left column, first row: sketch of nonlinear multi-mode $\chi^{(2)}$ optical processes that demonstrate the deterministic implementation of large CV networks and mode-dependent multi-photon subtraction. Second row: circuit representation of the two processes. Third row: graphical representation of the so-called cluster states (imprinted networks) where the nodes are the different modes of the field and edges correspond to C_Z gates between modes. Last and fourth row: emergent networks where edges are photon-number correlations between modes. Right column: same as left but considering imprinted cluster with shapes typical of complex network models.

C. Summary of the results

The entangling C_Z -gates in the imprinted network generate short range correlations between nodes. Also, the non-Gaussian operations we consider here - photon-subtractions - are applied locally on a single node. Under such conditions the effect of photon subtraction on a regular graph is limited [58]. On the contrary, here we probe imprinted graphs constructed from complex network models, where typical distances between nodes are short. Our results are as follows:

- For imprinted complex networks we see highly connected emergent networks of photon-number correlations. In such systems we show that photon-subtraction profoundly changes the structure of the correlation networks.
- We compare different complex network models, like Barabási-Albert or Watts-Strogatz, and their emergent correlation structure before and after subtraction of ten photons. The analysis of the distribution of degrees and clustering coefficients of the emergent correlation networks reveals that the amount of randomness of links or the inhomogeneity of number of links in different network models affects

the emergent correlation networks, before and after the photon subtraction. We see that some networks are more efficient than others in spreading the non-Gaussian effect.

- We show that photon subtraction generally affects the bulk clustering and degree distributions in the same way: it increases the mean and variance. This is in contrast with the structure in the tails of the distributions, characterized by higher moments, where the effect of photon subtraction is governed by the specific structure of the imprinted network.
- We unveil the importance of the local network structure in the vicinity of the node of photon subtraction. It is the connectivity of the imprinted sub-network spanned by this node and its neighbors that drives the changes due to photon subtraction.

D. Structure of the Paper

The Article is outlined as follows. Section II introduces the basic concepts of complex networks and CV cluster states used in this work to make the Article accessible to readers with different backgrounds – readers with

one or both areas of expertise may choose to skip this section or particular subsections. We describe the imprinted network structure and review non-Gaussian operations and their importance for getting non-Gaussian CV cluster states. We introduce the emergent correlation networks and complex network measures. Then in Sec. III we look at emergent correlation networks for Gaussian cluster states when different complex network models are used for the imprinted network. This section forms a baseline for the ensuing non-Gaussian analysis. In Sec. IV we describe the evolution of the emergent correlation networks when repeated photon subtractions are applied on the highest connected node vs. a random node. In Sec. V we show the influence of the subnetworks formed by nodes at fixed distance from the subtracting point, on the statistics in different non-Gaussian graphs. We then reveal the driving mechanism for the sub-networks at distance one. Finally, in Sec. VI we comment on general features of non-Gaussian correlations in photon-subtracted networks and specific features dependent on the imprinted network model.

II. QUANTUM COMPLEX NETWORK THEORY AND CONTINUOUS VARIABLE QUANTUM SYSTEMS

Networks are a collection of nodes and links. This is a very versatile conceptual structure that can be applied to any kind of relation between a collection of physical systems: receivers and senders in an information network linked by physical channels; atomic spins interacting via magnetic forces; or physical observables linked by correlation relations. Modern complex network theory in the physical, social, and life sciences is built on graph theory from mathematics and computer science. The adjacency matrix is the central mathematical object of complex network theory: a non-zero term in the matrix indicates a link between two nodes, where the indices of the matrix determine the nodes. All that is done in this Article can thus be understood as constructing the adjacency matrices for relevant networks, and subsequently extracting relevant properties from them.

In quantum information, graphs define the structure of the so-called graph or cluster states [59]. They correspond to multipartite quantum states with a specific entanglement structure introduced in the context of measurement-based quantum computing [56, 57, 60, 61]. For such cluster states, a non-zero term in the adjacency matrix indicates that an entangling gate has been applied between two qubits or between two quantum fields in two different optical modes (where the information is encoded in discrete or continuous variables, respectively). In this section we first provide a brief introduction to CV quantum optics in II A and we review the CV cluster states that are induced by the imprinted networks in Sec. II B. Then in Sec. II C we introduce the photon sub-

traction operation that creates non-Gaussian features in these quantum states. We define the emergent network of photon-number correlations in Sec. II D. Finally, in Sec. II E we review network measures in the context of complex network models.

A. Continuous variable quantum optics

The field of quantum optics can be seen as the study of the quantized light field, described by the electric field operator

$$\hat{E}(\vec{r},t) = \sum_{k=1}^{m} \mathcal{E}_k \hat{a}_k u_k(\vec{r},t). \tag{1}$$

The quantities $u_k(\vec{r},t)$ are an orthogonal basis of optical modes, i.e. normalized solutions of Maxwell's equations. \mathcal{E}_k is the electric field of a single photon in the mode k. Finally, the quantum features of the system are generated by the operators \hat{a}_k , which obey the commutation relation $[\hat{a}_j,\hat{a}_k^{\dagger}]=\delta_{j,k}$. Thus, every optical mode effectively is a quantum harmonic harmonic oscillator. In the CV framework, we focus on "position" and "momentum" variables of these harmonic oscillators, $\hat{x}_k=\hat{a}_k^{\dagger}+\hat{a}_k$ and $\hat{p}_k=i(\hat{a}_k^{\dagger}-\hat{a}_k)$, also called quadratures.

Generic quantum states of such quantum harmonic oscillators are hard to characterize, but the subclass of Gaussian states is very well understood. These states are completely described by the quadrature expectation values (the mean field) and covariance matrix V. To define the latter, let us introduce the 2m-dimensional vector $\vec{\xi} = (\hat{x}_1, \dots, \hat{x}_m, \hat{p}_1, \dots \hat{p}_m)^T$, and introduce

$$V = \operatorname{Re} \langle \hat{\xi} \, \hat{\xi}^T \rangle - \langle \hat{\xi} \rangle \langle \hat{\xi}^T \rangle, \tag{2}$$

where $\langle . \rangle$ denotes the expectation value of the observables in the state ρ . If this state is Gaussian, all its higher order correlations can be expressed in terms of V [62] (note that this property is explicitly used in Appendix A).

Changes in the mode basis $u_k(\vec{r},t)$ also induce changes in the quantum state description of the harmonic oscillators [63]. In this work, we will associate specific optical modes with the nodes of a network, as shown in Fig. 1. Such networks are naturally realized in the cluster state formalism of CV measurement-based quantum computing. It was experimentally demonstrated that such cluster states can be generated in arbitrary shapes [23].

B. Clusters: imprinted quantum networks

In the CV framework, cluster states are theoretically built starting from a set of modes of light prepared in the zero-momentum eigenstate $|0\rangle_p$, with $\hat{p}|0\rangle_p = 0$. The C_Z operators that serve as entangling gates have the form $C_Z = \exp(i\hat{x}_i \otimes \hat{x}_j)$ where \hat{x}_i is the position quadrature

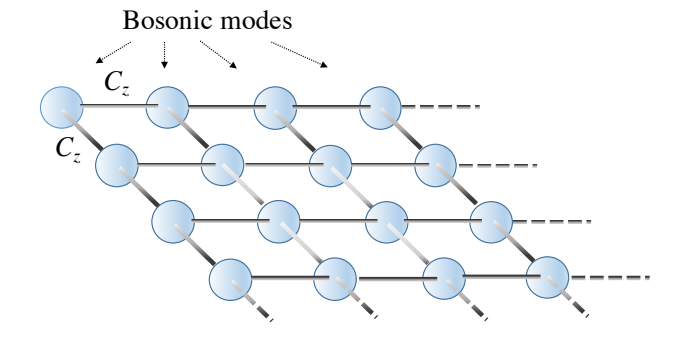


FIG. 2. Network representation of a two dimensional quantum cluster state, here pictured as a network where the nodes represent the bosonic modes and the links represent C_Z operations between pairs of nodes.

operator of the mode i, and likewise with j. As sketched in Fig. 1, the cluster state is built according to its adjacency matrix A as

$$|\Psi_C\rangle = \prod_{1 \le i < j < N} \exp(i\mathcal{A}_{ij}\hat{x}_i \otimes \hat{x}_j)|0\rangle_p^{\bigotimes N}.$$
 (3)

However, in quantum optics, momentum eigenstates such as $|0\rangle_p$ require infinite energy which cannot be achieved in any realistic experiment. It is therefore common to consider approximate cluster states, where $|0\rangle_p^{\bigotimes N}$ is replaced by a state that has finite squeezing in the \hat{p} -quadrature, i.e. a reduction below the vacuum noise of the expectation value of the variance of the p quadrature around 0. It is $\hat{S}(s)|0\rangle_{N}^{\bigotimes N}$, where $\hat{S}(s)$ is the squeezing operator, and $|0\rangle$ the vacuum state. The parameter s>1 denotes the squeezing, which for simplicity is chosen to be the same in all N copies.

This results in a Gaussian state with covariance matrix (2) given by $V_s = \mathrm{diag}[s,\ldots,s,1/s,\ldots,1/s]$. The first N elements in the diagonal are the variances of the x quadrature of the N modes (nodes) $\langle \hat{x}_i^2 \rangle = s \langle \hat{x}^2 \rangle_v = s$ where $\langle x^2 \rangle_v$ is the variance of the quadrature for the vacuum state which is taken equal to 1. The last N elements are the variances of the p quadrature $\langle \hat{p}_i^2 \rangle = 1/s$ of the N modes. The approximate cluster state that results by acting on $\hat{S}(s)|0\rangle^{\bigotimes N}$ with a network of C_Z gates is then described by [64]:

$$V = \begin{pmatrix} V_{xx} & V_{xp} \\ V_{px} & V_{pp} \end{pmatrix} = \begin{pmatrix} \mathbb{1} & 0 \\ \mathcal{A} & \mathbb{1} \end{pmatrix} V_s \begin{pmatrix} \mathbb{1} & \mathcal{A} \\ 0 & \mathbb{1} \end{pmatrix}$$
$$= \begin{pmatrix} s\mathbb{1} & s\mathcal{A} \\ s\mathcal{A} & s\mathcal{A}^2 + \mathbb{1}/s \end{pmatrix} \tag{4}$$

Here, V is a $2N \times 2N$ matrix divided into four $N \times N$ blocks. V_{xx} and V_{pp} describe the correlations among the x- and p-quadratures, respectively, whereas V_{xp} and V_{px} contain all correlations between x- and p-quadratures. The presence of \mathcal{A}^2 in V_{pp} highlights that correlations extend not only between nearest neighbor nodes, but also between next-nearest neighbors of the imprinted net-

work. The elements $[\mathcal{A}^2]_{ij}$ are in fact known to correspond to the number of walks of exactly two steps from j to i of the network \mathcal{A} [57, 58].

The C_Z gates, which create the entanglement, can be implemented according to any network shape, i.e., any adjacency matrix A. When used in measurement-based quantum computing, cluster states are built to ensure persistence of entanglement [65]. This means that a measurement on one node only locally affects the state and the surviving entanglement links can be further exploited for the next steps in measurement-based computing. To this end, some regular 2D graph structures, e.g., hexagonal or triangular lattices, have been proven to allow for universal computing. That is, arbitrary unitary operations can be performed via local operations and classical communication on the cluster. In contrast, others have been discarded, e.g. the tree graph [66]. Here we go beyond such regular structures, motivated by the fact that CV quantum networks in optical setups can be easily reconfigured to arbitrary shapes [23]. We want to indeed replicate in the quantum regime some of the models that mimic real-world complex networks [24, 25] in order to test their structural properties under local operations. In the remainder of the Article we refer to the network that describes the pattern \mathcal{A} of C_Z gates that are applied to create the Gaussian cluster state as the imprinted network.

C. Non-Gaussian operations in continuous variable platforms

Cluster states are characterized by Gaussian statistics of quadrature measurements, which allows for a compact statistical description even when they have a large size. However, for quantum computing protocols, cluster states must also acquire non-Gaussian quadrature statistics via non-Gaussian operations. Unlike the Gaussian case, the quantum features of such non-Gaussian networks are not trivial to classify [58, 67, 68]. Examples of non-Gaussian operations are the conditional implementation of single-photon subtraction and addition, i.e. the action of annihilation and creation operators \hat{a} and \hat{a}^{\dagger} [14, 15, 69–73]. Such operations have long been investigated as primitive for two important operations for quantum protocols: entanglement distillation and the generation of Wigner negativity. It can indeed be necessary to recover, via distillation [74–76], entanglement between nodes of a lossy and noisy network if we want to exploit it to teleport quantum states with large enough fidelity. On the other hand, the negativity of the Wigner function, one of the possible phase-space representations of the quantum state, is considered of the main signatures of the state's intrinsic quantum nature. When negative, we can no longer interpret it as a classical probability density [77] and it is considered a pivotal quantum resource in quantum information protocols [18, 78, 79]. Single-photon subtraction and

addition can also be combined to engender high-order non-Gaussian operations [17, 19, 80, 81].

In this Article, we focus on multi photon-subtraction operations that can ideally be represented, in a multimode case, by the following operation on a state ρ :

$$\rho \mapsto \frac{\hat{a}_{S_n} \dots \hat{a}_{S_1} \rho \hat{a}_{S_1}^{\dagger} \dots \hat{a}_{S_n}^{\dagger}}{\operatorname{tr}[\hat{a}_{S_1}^{\dagger} \dots \hat{a}_{S_n}^{\dagger} \hat{a}_{S_n} \dots \hat{a}_{S_1} \rho]},\tag{5}$$

where S_i denotes a particular mode. In general, Eq. (5) describes repeated subtractions from different nodes, or even from superpositions of different nodes, that have recently been experimentally implemented [14, 69]. When these operations are applied on multimode quantum states, like the cluster state in Eq. (3), characterization of the resulting states is not a trivial task. Recent results have depicted the rules of thumb for entanglement and Wigner negativity [16, 58, 67, 68], indicating that a deeper structural analysis would be beneficial for a more comprehensive picture.

Here, we specifically consider repeated photon subtractions from one single node of the cluster state in Eq. (3) are identical. There are two main reasons for this choice. First, we focus on the simplest scheme providing significant statistics. In fact, when multiple subtraction from an arbitrary superposition of nodes is considered, the analysis becomes computationally hard [22]. Second, we aim at probing the extent of the effect of photon subtraction in the most local way possible. In previous work, we have shown that photon subtraction on a given node induces non-Gaussian features in its nearest and next-nearest neighbor nodes [58]. This Article goes beyond single-point features such as local averages. Instead, we focus on the changes induced in the correlations between those nodes, including beyond next-nearest neighbors. We then study how different imprinted network shapes A spread or destroy the non-Gaussian features created by photon subtraction. This is a problem that is very typical for classical information networks, studied here in the new context of quantum correlations.

D. Emerging complex networks of photon number correlations

Covariance matrices are sufficient to explain the behaviour of Gaussian states. In the case of non-Gaussian states expectation values of higher order operators are needed. In this Article, we focus on photon-number correlations, that are among the simplest non-Gaussian observables with a clear physical interpretation. Photon number correlations can be written in terms of quadrature correlations. The expression will then involve fourth moments of quadratures, which are sensitive to the non-Gaussianity – i.e., departure from Gaussian shape – of the quadrature distribution [16]. Moreover, photon-number correlations are extensively used to study features of non-Gaussian processes in quantum optics, such

as Hong-Ou-Mandel interference [82], photon bipartite entanglement [83], and photon distinguishability [84]. They also serve to benchmark single-photon sources [85], n-photon sources [86], and quantum protocols such as boson sampling [87, 88].

To consider structural effects, we introduce a second network for each cluster state, composed by the emergent structure of photon-number correlations between pairs of modes. As such, we define the correlation matrix \mathbb{C} :

$$[\mathbb{C}]_{ij} = \frac{|\langle \hat{n}_i \hat{n}_j \rangle - \langle \hat{n}_i \rangle \langle \hat{n}_j \rangle|}{\sqrt{(\langle \hat{n}_i^2 \rangle - \langle \hat{n}_i \rangle^2) \left(\langle \hat{n}_j^2 \rangle - \langle \hat{n}_j \rangle^2\right)}},\tag{6}$$

where we take the absolute value of the correlation, since we are purely interested in the strength of the correlation, rather than its sign. The values of $|\langle \hat{n}_i \hat{n}_j \rangle - \langle \hat{n}_i \rangle \langle \hat{n}_j \rangle|$ depends on the number of photons in the system; it may be higher for two weakly correlated nodes with very high photon numbers, than for strongly correlated nodes with very small photon numbers. Due to its conditional nature, photon subtraction locally changes the photon number in the system, thus making it impossible to genuinely compare the resulting values of $|\langle \hat{n}_i \hat{n}_j \rangle - \langle \hat{n}_i \rangle \langle \hat{n}_j \rangle|$ in the two cases. The denominator in Eq. (6) solves this problem by renormalizing the correlation to be confined between zero and one, where one implies that both nodes contain the same number of photons, regardless of how many photons there are.

Eq. (6) ultimately allows us to look at the correlation network, as given by its weighted adjacency matrix:

$$\mathbb{A} = \mathbb{C} - \mathbb{1}. \tag{7}$$

In the following we will characterize what kind of correlation networks (\mathbb{A}) emerge, in the same spirit of mutual information networks in [36], when photon-subtraction operations are applied on cluster states with different shapes \mathcal{A} . Hence, network structures are considered at two different levels: one is the imprinted network which describes the entangling gates that induce Gaussian entanglement between position and momentum in the cluster state of Eq. (3); the other is the emergent network of photon-number correlations defined in Eq. (7) via Eq. (6). This second network will be analyzed via measures and metrics typical of complex network theory, as we detail in the following in Sec. II E.

E. Complex network measures in complex network models

Quantitative measures of network structures have been introduced by network theory [27, 28]. From the adjacency matrix components we can calculate the degree D_i for each node i, i.e., the number of links connected to it, as

$$D_i = \sum_j \mathbb{A}_{ij}.$$
 (8)

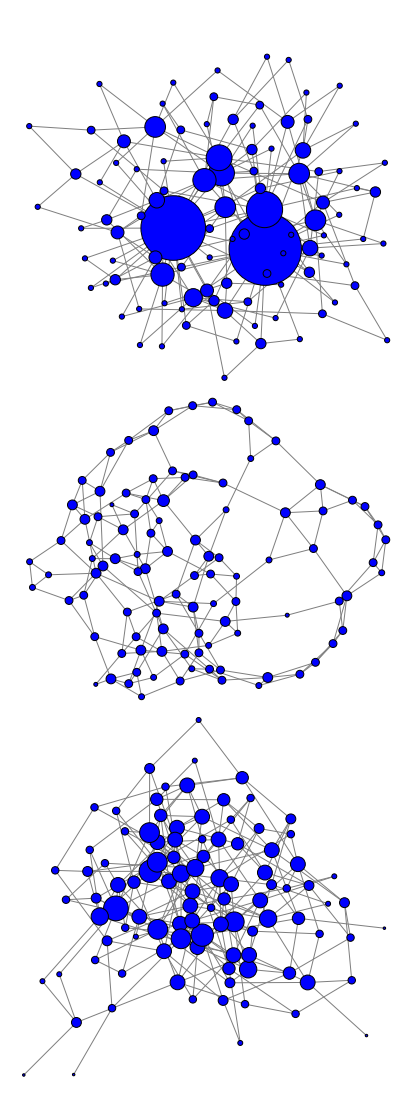


FIG. 3. Three complex networks of 100 nodes. Top: Barabási-Albert (BA) network built via preferential attachment with m=2 nodes added at each step. Middle: Watts-Strogatz (WS) network built via rewiring, with probability $p_{\rm WS}=0.2$, a regular network with degree per node d=2. Bottom: Erdos-Renyi (ER) network with connection probability $p_{\rm ER}=0.04$. The size of the nodes is proportional to their degree.

The degree distribution p(D) gives the probability for a random node to have the degree D. Even if is not possible to get the full information on the structure of a network by its degree distribution, it can be informative to look at the shape of the distribution. Similarity arguments between different real-world networks have been based in part on analogy between their degree distributions, which often follow a power-law rule. Moreover, many crucial properties of networks, like their robustness to perturbations and the spread of contamination, are determined by the functional p(D) [28].

A second quantitative measure of complexity is the local clustering coefficient. It gives information on the connections between the neighbors of a specific node, thus keeping track of local correlations around a point. A common way of defining the clustering coefficient is the number of triangles to which the node belongs divided by the number of triplets. It can be recovered from $\mathbb A$ as

$$Cl_i = \frac{\sum_{j \neq k} \mathbb{A}_{ij} \mathbb{A}_{jk} \mathbb{A}_{ki}}{\sum_{j \neq k} \mathbb{A}_{ij} \mathbb{A}_{ik}}$$
(9)

for $i \neq j \neq k$.

Here we briefly review some of the paradigmatic models that have been proposed for real-world networks: the random network model called Erdős-Rényi (ER), the Barabási-Albert (BA) model and the Watts-Strogatz (WS) model. The ER model builds networks by randomly connecting nodes according to a uniformly random probability $p_{\rm ER}$ for two nodes to be connected. The resulting networks exhibit a binomial distribution of links per node. The ER model is able to reproduce the typical average shortest path distances between nodes of real networks.

A second model that has been introduced to reproduce typical complexity signatures of real networks is the BA model. It describes network formation processes based on the preferential attachment model: the network grows by adding new nodes. These new nodes attach with m links to old nodes. The probability of connection is proportional to the degrees of the existing nodes, such that the highest degree nodes are the preferred ones. This model is able to reproduce the power-law distribution in the degree, and thus the existence of "hubs", i.e., nodes with very large degree, as in real-world networks.

Finally, the WS model is able to reproduce the small-world mechanism, where any node is a short path from any other in the network. Specifically, the distance between any two nodes grows as the log of the total number of nodes. It is built by starting from a regular network in which each vertex has a fixed degree k; for instance, k=2 would correspond to a lattice in tight binding approximation. Then nodes are rewired according to a probability $p_{\rm WS}$. One interesting feature of this model is that it allows one to tune continuously from regular $(p_{\rm WS}=0)$ to random $(p_{\rm WS}=1)$ networks.

When the complex networks model will be used in the remainder of this Article, in order to achieve reasonable statistics, we will consider many realisations of networks made of 100 nodes for each model, and different parameters within each model. These are quite small networks when compared with typical real-world networks, but even for this small scale the different models exhibit visibly different features. In Fig. 3, we show a BA network built by adding m=2 new nodes at each step in network growth from 2 nodes to 100; a WS network built starting from a regular network with degree per node $k = \langle D \rangle = 2$ and rewired with a probability $p_{\rm WS}=0.2$; and an ER network with connection probability $p_{\rm ER} = 0.04$. One observes clear differences between the three networks, with, for example, the emergence of easily visible hubs in the BA model, shown as large blue

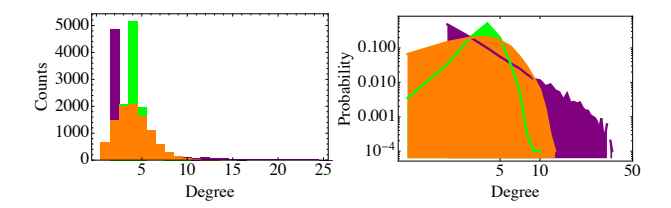


FIG. 4. Histogram of the degree distribution for 100 networks of the three types shown in Fig. 3, BA (purple), WS (green), ER (orange). On the left the linear scale is used while on the right the scale is double-logarithmic to emphasize the appearance of the power-law tail for the BA networks. The average degree is $\langle \mathcal{D} \rangle = 4.44$ (BA), 4.0 (WS) and 4.09 (ER).

discs in the figure. By taking 100 network realizations for each model one observes that the resulting degree distribution, shown in Fig. (4), is distinct in the three cases, even if they have similar average value. In particular, the logarithmic scale shows the power-law distribution for the BA networks.

In the following, we choose particular network models to shape the adjacency matrix $\mathcal A$ of the imprinted networks. In the rest of the paper we will consider only the BA and WS models as the ER network shows very similar features as the WS models with high rewiring probability $p_{\rm WS} \to 1$. With the probabilistic generation of a statistically significant number of networks for each model, it will be possible to reveal specific features, in this case quantum ones, that are determined by the structure of the network.

We want to stress that the network models we have chosen are a very limited set of the ones that have been developed in complex network theory. The ones we selected have specific features - in particular: variable level of randomness, presence of hubs, power law distribution, and average short path distances - that have never been tested before in non-Gaussian cluster states. Of course other models and features can be treated in future works.

III. EMERGENT NETWORKS IN COMPLEX GAUSSIAN CLUSTER STATES

In this section, we explore how the network topology of the imprinted network influences the properties of the emergent network before any photon subtraction. The quantum state in such Gaussian networks exhibits Gaussian statistics. The results of this section then form a baseline from which to compare the effect of photon subtraction on networks in Sec. IV and Sec. V.

The imprinted networks are obtained by applying C_Z gates to a set of squeezed vacuum modes according to an adjacency matrix \mathcal{A} for the BA and WS models defined in Sec. II E. We then directly examine the emergent network with adjacency matrix \mathcal{A} . Throughout all our simulations, we fix the amount of squeezing to 15dB (i.e., $s \approx 31.6$ units of shot noise) for each squeezed vacuum

mode.

As described in Sec. IIB, the correlation between quadratures of different modes goes beyond the graphical structure imprinted by the C_Z gates, as quadrature correlations appear not only between nearest neighbours but also between next-nearest-neighbor correlations. So even before photon subtraction the emergent networks of photon number correlations, that inherit quadrature correlations, are different from the imprinted networks, but with very specific features that depend on the imprinted networks. The calculation of photon number correlations for the cluster before photon subtraction can be carried out analytically by using the techniques of Appendix A. We obtain the weighted adjacency matrix (as derived in Appendix A 2)

$$[\mathbb{A}]_{ij}^G = \frac{\frac{s^2}{8}(([\mathcal{A}^2]_{ij})^2 + 2\mathcal{A}_{ij})}{\sqrt{\mathfrak{N}(s, \mathcal{D}_i)\mathfrak{N}(s, \mathcal{D}_i)}} - \delta_{i,j}, \tag{10}$$

where $\mathfrak{N}(s, \mathcal{D}_k) = (s^2 + 1/s^2 + s^2(\mathcal{D}_k)^2 + 2\mathcal{D}_k - 2)/8$ is a normalization factor depending only on the initial squeezing value s and the degree \mathcal{D}_k of the node k in the imprinted network. Recall from Sec. II B that $[\mathcal{A}^2]_{ij}$ is the number of different walks of exactly two steps that connect nodes i and j in the imprinted structure. Therefore, the links between nodes i and j in the emergent network are non-zero if either i and j are connected in the imprinted network $(\mathcal{A}_{ij} = 1)$ or when they are nextnearest neighbors $([\mathcal{A}^2]_{ij} \neq 0)$.

Hence, we can already anticipate an important difference in number of links in the emergent networks of photon number correlations when we move from the traditional regular structures used for clusters (like grid shapes) to imprinted networks with complex network structure. In the latter, the number of walks of distance two between different nodes is in general larger as compared to regular networks.

A. Barabási-Albert networks – Emergent triangles and clustering

The imprinted BA networks have a multitude of weakly connected nodes that are organized around a few highly connected hubs. We collect statistics of 100 different networks of 100 nodes both for the parameter m = 1 (e.g. top row of Fig. 5) and for m=2. From the example in Fig. 5, we immediately observe the differences in number of links in the emergent network when compared to the imprinted network, even though the rough outline of the network remains similar. The BA network with m=1 is an excellent example to illustrate the difference: this imprinted network has a tree-like structure, which implies that many nodes have only one connection. In the emergent network, however, all nodes have at least two connections due to what we discussed above, i.e., the presence of walks at distances two in the imprinted network. A more quantitative understanding is acquired from the

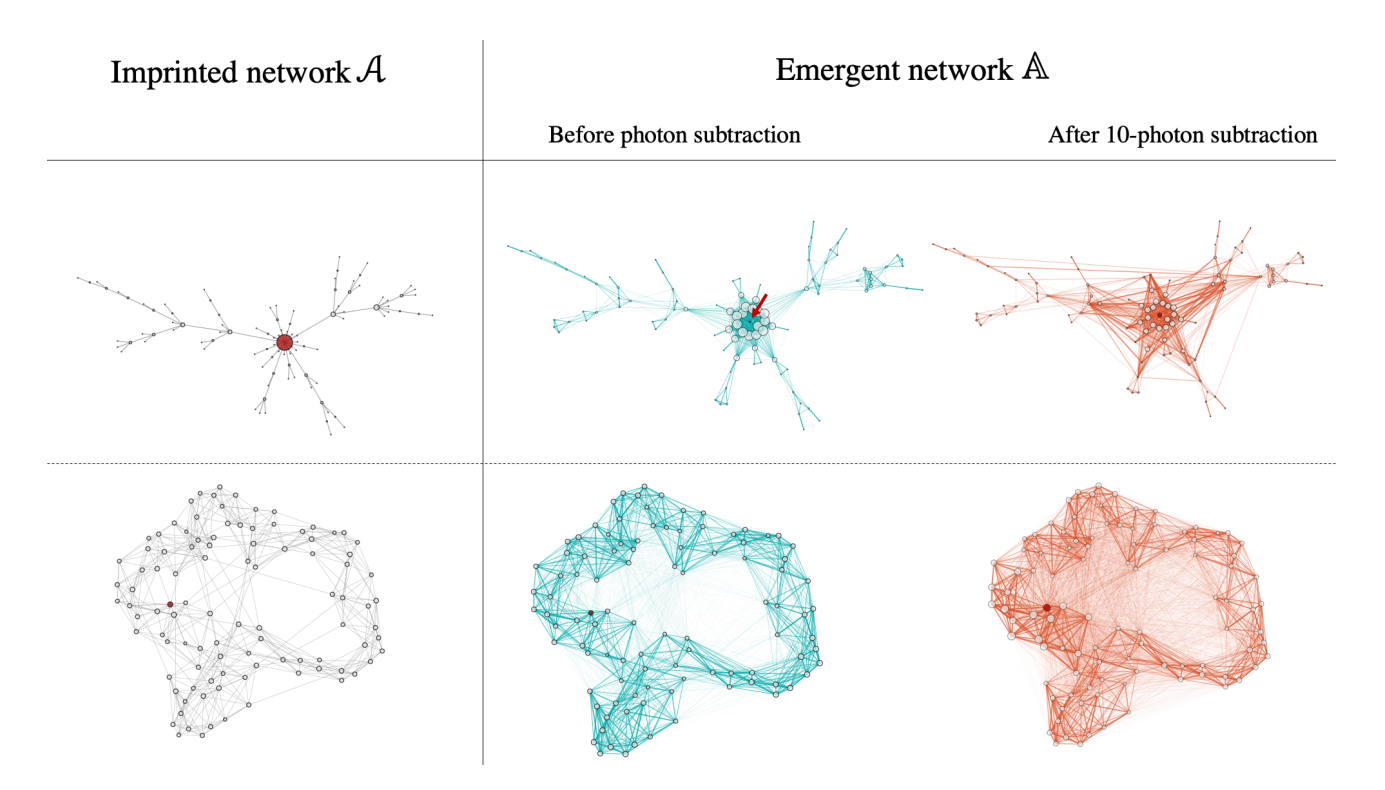


FIG. 5. Imprinted networks \mathcal{A} (left column) give rise to emergent networks \mathbb{A} (middle column), which can then further undergo photon subtraction (right column). Photon subtraction at indicated red node; node sizes show the degree. Imprinted networks include Barabási-Albert with m=1 (top row) and Watts-Strogatz generated from a regular one-dimensional network in which every node is connected to its k=5 nearest neighbors with a rewiring probability $p_{\text{WS}}=0.05$ (bottom row).

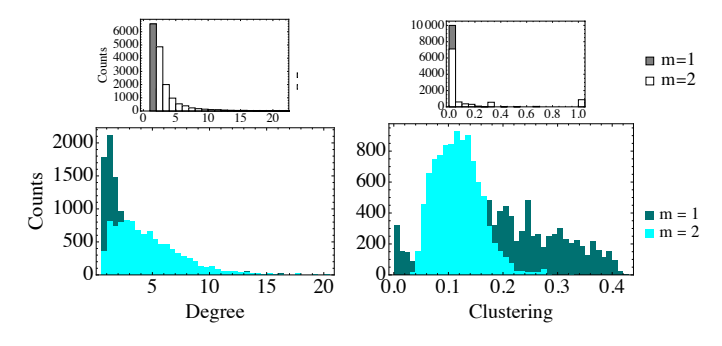


FIG. 6. BA emergent network statistics in Gaussian case. Histogram of degree and clustering for the imprinted BA network with m=1 and m=2 (top row) and associated emergent network of photon number correlations (bottom row) in the Gaussian case, i.e., when no photon is subtracted.

histograms of the degree and clustering coefficients in the emergent network of Fig. 6 for m=1,2 in comparison with the original distribution of the imprinted network. The emergent degree distributions inherit the features of the imprinted network, with a small number of nodes with high degrees, although with larger variances. In contrast, the histogram of clustering is dissimilar to the clustering in the imprinted network. In particular, for m=1 the imprinted network does not have any triangles, and thus clustering is zero for all nodes while the

emergent correlation network has non-zero values quite uniformly distributed but only in the range of 0.0 - 0.4.

B. Watts-Strogatz networks – More randomness for lower degree and clustering

As mentioned in the introduction to complex networks of Sec. II E, WS networks are highly tunable and versatile. In particular, in the limit of a vanishing rewiring probability we recover a completely regular network, whereas in the limit of high rewiring probability the network closely resembles an ER network. In our simulations, we start from a regular one-dimensional network with 100 nodes, each of which is connected to 2k other nodes. This network can be represented by organizing the nodes in a circle, where every node is connected up to its $k^{\rm th}$ neighbor. Subsequently we rewire the connections with probability $p_{\rm WS}$. For various choices of $p_{\rm WS}$, we implemented 100 of these WS networks as imprinted structures to apply C_Z gates [89]. As for the BA case we look at the statistics of degree and clustering.

The bottom row of networks in Fig. 5 shows a typical realization of a WS network with k=5 and $p_{\rm WS}=0.05$. The imprinted network is therefore reasonably close to a regular network in which each node has 2k=10 connections. We observe that the emergent network before photon subtraction, with a weighted adjacency matrix \mathbb{A} ,

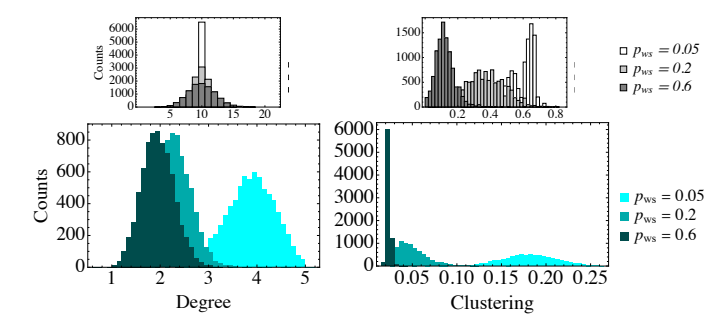


FIG. 7. WS emergent network statistics in Gaussian case. Histogram for the degree and clustering for the imprinted networks (top row) and for the emergent network of photon number correlations in the Gaussian case (when no photon is subtracted) (bottom row). Here results on the WS network model with $p_{\rm WS}=0.05,0.2$ and 0.6 are reported.

has a richer and more varied structure in its connections. Nevertheless, we can still see a qualitative resemblance between the imprinted and the emergent network.

In Fig. 7 we examine the difference in degree and clustering coefficient between imprinted and emergent networks. We observe that the properties of the imprinted WS networks strongly influence the structure of the emergent correlation networks. The degree distribution for the imprinted networks is always centered around 2k = 10 with larger variances for larger p_{WS} . The degree distributions for the emergent networks are centered around different mean values for the three $p_{\rm WS}$ cases. The $p_{WS} = 0.05$ case shows a broader and more skewed distribution of significantly higher degrees. Hence, for the emergent networks, in contrast to the imprinted ones, the largest variance is for the lowest p_{WS} . In general, we conclude that an increased probability of rewiring (and thus more randomness) in the imprinted network decreases the degree (which is essentially the total amount of correlation of every node) in the correlation network of Gaussian clusters.

This reduction in the degree should be explained by a reduction in the weight of the connections because, from (10), we can demonstrate that the number of connection in the emergent network is higher for larger values of $p_{\rm WS}$. This is related to the choice of the normalization given by the denominator in the elements of the correlation matrix, as explained in Sec. II D. The histogram for the clustering coefficient is qualitatively similar to that of the degree, in the sense that increased rewiring leads to a decrease in clustering, and it is also very similar to the clustering of the imprinted networks.

IV. THE EFFECT OF NON-GAUSSIAN STATISTICS ON EMERGENT NETWORKS

In this section we study the effect of photon subtraction, introduced in Sec. II C, on the emergent network of photon-number correlations. Because the operation

is locally applied on a single node in the imprinted network, one might consider this to be a single-node attack, as in classical complex network theory. However, we emphasize that no nodes are removed in the photon subtraction process. So it is not a single-node attack in the classical sense. In quantum networks, operations like node removal or link shortening have to be introduced in the context of cluster states via Gaussian (homodyne) measurements [57]. Quantum complex networks have a large variety of attacks, i.e., modifications to the network structure and properties, as compared to classical networks. Here we are not interested in modifying the size or the shape of the imprinted cluster by operations such as node removal, but we instead want to analyze the spreading of non-Gaussian correlations in cluster states when affected by photon subtraction in one node.

Repeated photon subtraction in the same node is expected to increase correlations in the system due to entanglement distillation [90]. Moreover, from the results in [67], we can deduce that photon subtraction in a given node creates correlations between previously uncorrelated nodes. However, it is not understood a priori how the topology of the imprinted network influences the effects of photon subtraction(s) on the topology of emergent correlation network. To address these questions, we investigate the effect of subtracting ten photons, on the distributions of the degrees and clustering coefficients for the emergent networks. An overview of the path followed in our network analysis can be found in Fig. 8. In the remainder of the Article we will explain each one of these steps in detail.

The number of photons to be subtracted (ten) is chosen to have a large effect in the emergent network, although we do not find qualitatively different results for somewhat larger or smaller numbers of subtracted photons. However, increasing the amount of squeezing in the initial imprinted network or the number of photon subtractions does quantitatively enhance the observed features.

To study the effect of photon subtraction, we first provide analytical results on the reach of the effect of photon subtraction. Then, we compare the qualitative features that are seen in the histograms of numerically generated distributions of degrees and clustering coefficients. To get a complementary quantitative view, we perform a moment analysis and probe the effect of the non-Gaussian operation on the mean, variance, skewness, and kurtosis. Readers unfamiliar with these quantities can find their definitions in Appendix C.

A. The effect of photon subtraction is strictly local

The subtraction of a single photon subtraction in a cluster state is know to only affect vertices in the vicinity of the node of subtraction [58]. In Appendix B, we extend this understanding to the correlations between observ-

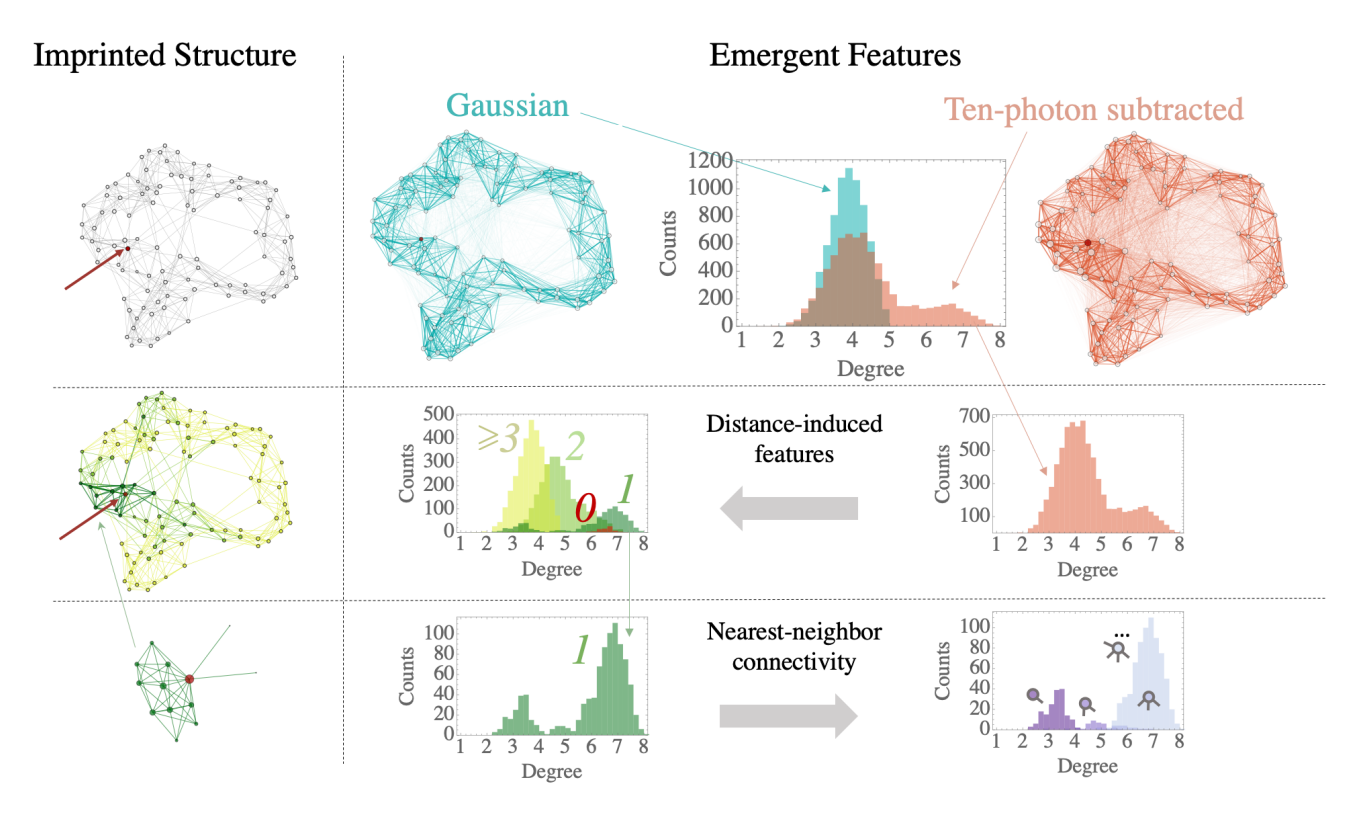


FIG. 8. Analysis and structures for an imprinted WS network. Generated from a regular one-dimensional network in which every node is connected to its k = 5 nearest neighbors with a rewiring probability $p_{\rm WS} = 0.05$. Top row: imprinted complex network (left, node with highest degree is highlighted in red); and emergent networks before subtraction (Gaussian, middle) and after subtraction (Ten-photon subtracted, right) with their corresponding degree distributions. Middle row: degree distribution of the photon-subtracted case (zoom on right) is broken up, in the central panel, according to the distance $(0, 1, 2, \text{ or } \geqslant 3)$ of nodes from the subtraction node. The color code used for different distances is adopted for the nodes in the imprinted network (left). Lower row: Structure of the next-neighbor nodes (distance 1) is highlighted (left); zoom of the degree distribution at distance one (middle); statistics is broken up according to the connectivity of the different nodes (right).

ables that are defined on different regions of the system: the correlation $\langle \hat{X}\hat{Y} \rangle - \langle \hat{X} \rangle \langle \hat{Y} \rangle$ between two observables \hat{X} and \hat{Y} can only be influenced by photon subtraction when both observables have a support on modes that are correlated to the mode of photon subtraction. This result applies regardless the number of photons that are subtracted.

For the networks in this work, we subtract photons in one specific node. In the initial Gaussian state, Eq. (4) shows that this node is correlated to all nodes that are either nearest-neighbours (given by \mathcal{A}) or next-to-nearest neighbours (given by \mathcal{A}^2) in the imprinted network of C_Z gates. We label S the node of photon subtraction and denote the expectation value in the photon subtracted state $\langle \ldots \rangle$, whereas $\mathrm{tr}[\ldots \rho]$ is the expectation value in the Gaussian cluster state. Our general result of Appendix B then shows that $\langle \hat{n}_i \hat{n}_j \rangle - \langle \hat{n}_i \rangle \langle \hat{n}_j \rangle = \mathrm{tr}[\hat{n}_i \hat{n}_j \rho] - \mathrm{tr}[\hat{n}_i \rho] \mathrm{tr}[\hat{n}_j \rho]$ for all nodes i and j which satisfy the condition that either $\delta_{S,i} = \mathcal{A}_{S,i} = (\mathcal{A}^2)_{S,i} = 0$ or $\delta_{S,j} = \mathcal{A}_{S,j} = (\mathcal{A}^2)_{S,j} = 0$. More colloquially phrased, photon-subtraction in S only alters the value of $\langle \hat{n}_i \hat{n}_j \rangle - \langle \hat{n}_i \rangle \langle \hat{n}_j \rangle$ if either node i or node j is more than two steps removed from S in the imprinted network.

Looking back at Eq. (6), we must also consider the effect of photon subtraction on the denominator on the final emergent network. Let us assume that node i is within the vicinity of S, i.e., $\max\{\delta_{S,i}, \mathcal{A}_{S,i}, (\mathcal{A}^2)_{S,i}\} \geqslant 1$, but j is further away, i.e., $\delta_{S,j} = \mathcal{A}_{S,j} = (\mathcal{A}^2)_{S,j} = 0$. In this case, after photon subtraction in S we obtain the Gaussian value when we calculate $\langle \hat{n}_i \hat{n}_j \rangle - \langle \hat{n}_i \rangle \langle \hat{n}_j \rangle$. Likewise, we will find that $\langle \hat{n}_j^2 \rangle - \langle \hat{n}_j \rangle^2$ remains unaffected. However, because i is in the vicinity of S, we do find that $\langle \hat{n}_i^2 \rangle - \langle \hat{n}_i \rangle^2$ changes its value. In other words, photon subtraction will still have an effect on the emergent network as constructed via Eq. (6), unless $\langle \hat{n}_i \hat{n}_j \rangle - \langle \hat{n}_i \rangle \langle \hat{n}_j \rangle = \operatorname{tr}[\hat{n}_i \hat{n}_j \rho] - \operatorname{tr}[\hat{n}_i \rho] \operatorname{tr}[\hat{n}_j \rho] = 0$. From Eq. (10), we see that this implies that the effects of photon subtraction spread up to four steps in the emergent correlation network.

We therefore have proven that effects of photon subtraction in such a multimode system can only affect a certain environment around the node of subtraction. Moreover, the range at which photon subtraction is effective is independent of the number of subtracted photons. Hence, to study the effect of photon subtraction, we can

restrict ourselves to intermediate network sizes. For the types of networks and the parameter ranges we consider a choice of ~ 100 nodes guarantees that most nodes are no further than four steps from the point of subtraction. We are thus confronted with intermediate system sizes which may appear small to classical network scientists, but are far beyond the reach of any standard quantum optics techniques.

As we will show, the methods of complex network theory offer a new window to understand how photon subtraction influences the nodes within its range of effect.

This result also imposes another important conclusion: to induce non-Gaussian effects in vast cluster states, one must subtract photons in many different nodes. However, in Appendix A3, we argue how the complexity of this problem effectively makes it computationally very hard to simulate. From a physical point of view, one would subtract these photons by coupling a tiny amount of light from each node, in which we want to subtract, into an auxiliary mode. Then we need photon detectors on these auxiliary modes to fire at the same time. Already at this state preparation stage, we see connections to Gaussian boson sampling [91], where it is shown that simulating the clicks of photon detectors mounted on a sufficiently complicated Gaussian states is computationally intractable. Similarly, there is also a direct connection to the hardness of sampling continuous variables on a photon subtracted state [92]

On a mathematical level, the problem at the basis of the computational complexity of these sampling problems is the problem of finding perfect matchings [93]. As we argue in detail in Appendix A 3, the problem of finding all perfect matchings also appears when constructing the emergent network of photon-number correlations. Hence, fully simulating such networks in detail is only possible when many photons are subtracted in many modes.

Yet, when large states with photons subtracted in various modes are created in experiments, the measurement and analysis of emergent correlations networks may well turn out to be an important tool to characterise such states. Note that the same type of photon-number correlations have been used to benchmark computationally intractable Gaussian boson sampling experiments [94, 95].

B. Photon subtraction in Watts-Strogatz networks - More randomness for larger effects

To maximize the effect of photon subtraction we choose to always subtract the photon in the node with the highest connectivity in the imprinted network, i.e., the biggest hub. As such we probe network environments in the imprinted WS structure with the highest correlations. This choice has a small effect in the case of WS networks as most nodes have a similar connectivity, unlike BA networks where a few nodes serve as highly connected hubs.

In Fig. 9 we choose rewiring probabilities $p_{WS} =$

0.05, 0.2, 0.6 to probe the effect of different imprinted network environments on the degree distribution in the emergent network of photon-number correlations. The data for each value of p_{WS} are obtained by combining 74 random realizations of a 100-node network. The effect of photon subtraction is qualitatively similar in all cases. A subset of nodes in the photon-subtracted cluster states retains degrees of the same order of magnitude as for the Gaussian network state, whereas a second subset finds its degree considerably increased, resulting in a bimodal distribution. This qualitative similarity translates to the moments in Fig. 9(B), in the sense that photon subtraction shifts the distributions to higher means and variances, regardless of the value of p_{WS} . However, photon subtraction causes stronger increases in the mean and variance for larger values of p_{WS} , and the higher moments behave differently depending on p_{WS} . These features are observed in Fig. 9, where an increase in p_{WS} lowers the overlaps between the histogram before and after photon subtraction.

In Fig. 10, we explore the role of photon subtraction on the clustering coefficients. The observed difference between different values of $p_{\rm WS}$ is even more profound: the clustering coefficients are only weakly affected by photon subtraction for $p_{WS} = 0.05$, whereas for $p_{\rm WS}=0.6$ the histogram changes dramatically. These drastic changes are also seen when comparing the moments before and after photon subtraction in Fig. 10 B, where photon subtraction increases the skewness and kurtosis for $p_{WS} = 0.05$, but strongly decreases these moments for $p_{WS} = 0.6$. Nevertheless, even though the clustering coefficients are not strongly affected by photon subtraction in imprinted WS structures with $p_{WS} = 0.05$, these clustering coefficients remains much higher than those of the imprinted networks with higher values of $p_{\rm WS}$ (which one can also confirm in the moments).

These observations coincide with the intuition that photon subtraction generally increases the correlations in our system. However, it remains to understand which features of the network structure associated with the different values of $p_{\rm WS}$ determine the extent of the effect of photon subtraction.

Because low rewiring corresponds to more regular networks, it is interesting to compare the given results with the fully-connected (or complete) network, which is not only totally regular but also the one with the highest possible number of connections, n(n-1)/2. All the nodes then have the same degree and clustering. For the imprinted network these are respectively D=99 and Cl=1, whereas the emergent Gaussian networks yield D=97.019 and Cl=0.970086. After the subtraction of ten photons, we found D=97.037 and Cl=0.970649 for the node of subtraction and D=97.074 and Cl=0.970642 for all the others. The effect of photon subtraction in highly connected regular networks is tiny. Thus, such networks are less effective for spreading non-Gaussian correlations from a single local operation.

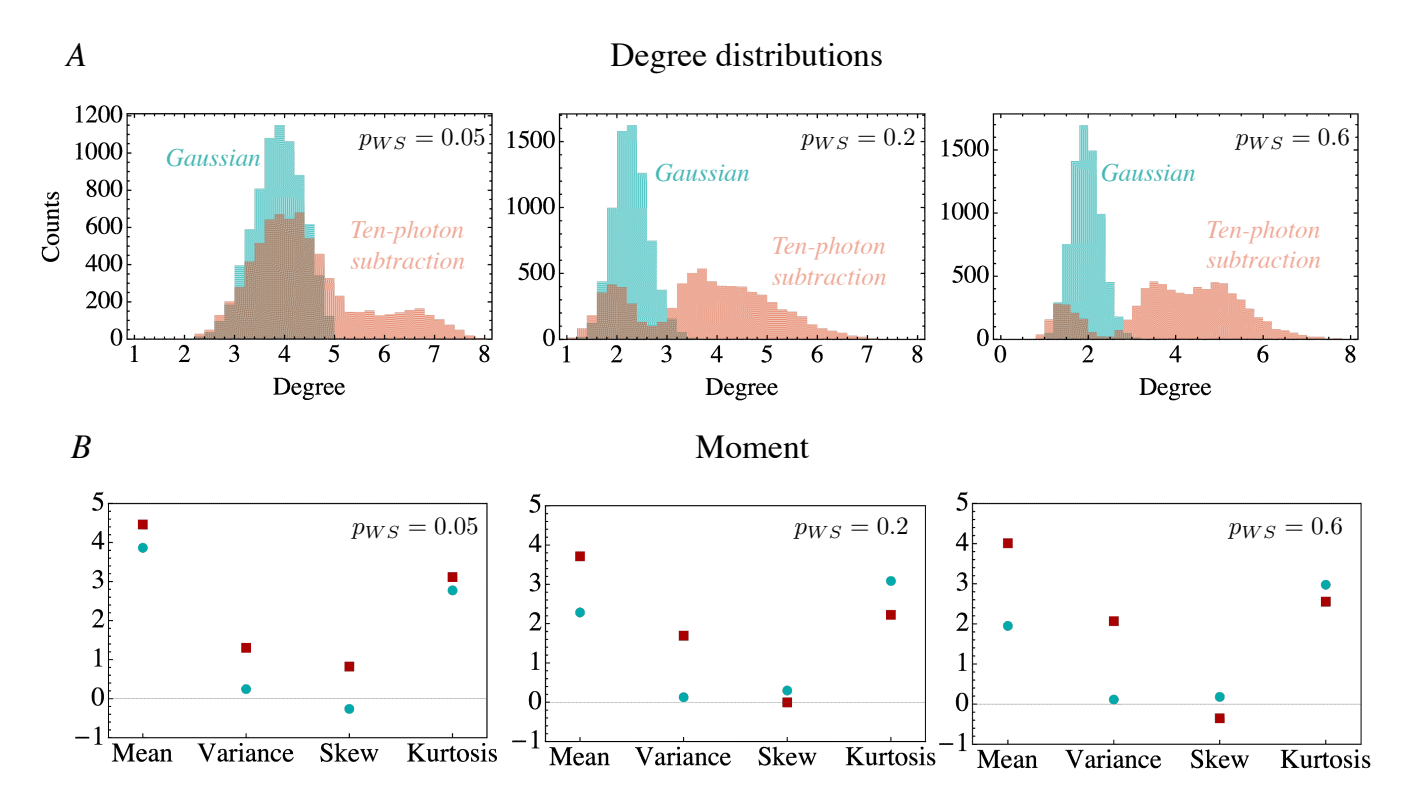


FIG. 9. Histograms (A) and moments (B) for the degree distributions of the emergent correlation network obtained from a WS imprinted structure with rewiring probabilities $p_{WS} = 0.05, 0.2$ and 0.6. Colors indicate degree data prior to (cyan, dots) and after (red, squares) the subtraction of ten photons in the node with the highest connectivity. Data were each obtained by combining 74 random realizations of a 100-node network. The WS imprinted network is obtained by starting from a one-dimensional regular network where each node is connected to its k = 5 nearest neighbors. Both moments and histograms show how photon subtraction changes the bulk of the distribution by increasing the mean degree and the width of the distribution (i.e., variance). The higher moments and histograms also show that the finer structure in the tails of the degree distribution depends strongly on the value of p_{WS} .

C. Photon subtraction in Barabási-Albert networks –Difference between random and highly connected subtraction node

We now explore how photon subtraction affects the emergent network of a BA imprinted structure, both when we subtract always in the most important hub (i.e., the node with the highest connectivity in the imprinted network), and when we subtract in a randomly chosen node (likely a node with low connectivity).

Even before photon subtraction the moment analysis in Fig. 11(B) shows that for imprinted BA structures the degree distributions of emergent correlation networks have a large variance and kurtosis, in particular for m=1. Hence, the emergent networks inherit some of the power-law features of the imprinted structures. In the top panels of Fig. 11 we therefore show the degree distribution on a log-log scale, for m=1 and m=2, before and after subtraction of ten photons.

For m=1 imprinted structures, the effect of photon subtraction manifests within the tail of the distribution. We observe the power-law behaviour that is suggested by the moments, and we find that photon subtraction in a

hub tends to reduce the weight in the tail. Thus, photon subtraction in the most important hub has a reasonably small effect on a large fraction of the network to make the degrees somewhat more homogeneous. In contrast, photon subtraction increases the weight in the tail if it occurs in a random node. This shows that, when the photons are subtracted in a node that is correlated to only a small number of other nodes, it can very significantly increase these correlations, thus causing larger values to appear in the tails. This behaviour is consistent with photon subtraction as a finite resource for entanglement distillation. Yet, it must me stressed that photon-number correlation are not necessarily quantum correlations. For nodes with a high connectivity, photon subtraction only weakly alters the individual correlations. As a final comment for the m=1 case, we must note that the bulk of the distribution remains largely unaffected, up to a point where the effect of photon subtraction is hardly visible when the histogram is plotted on a linear scale – this is also reflected by a relatively small change in the mean degree.

For m=2 imprinted structures, the distribution does not show typical power-law behaviour, which is reflected

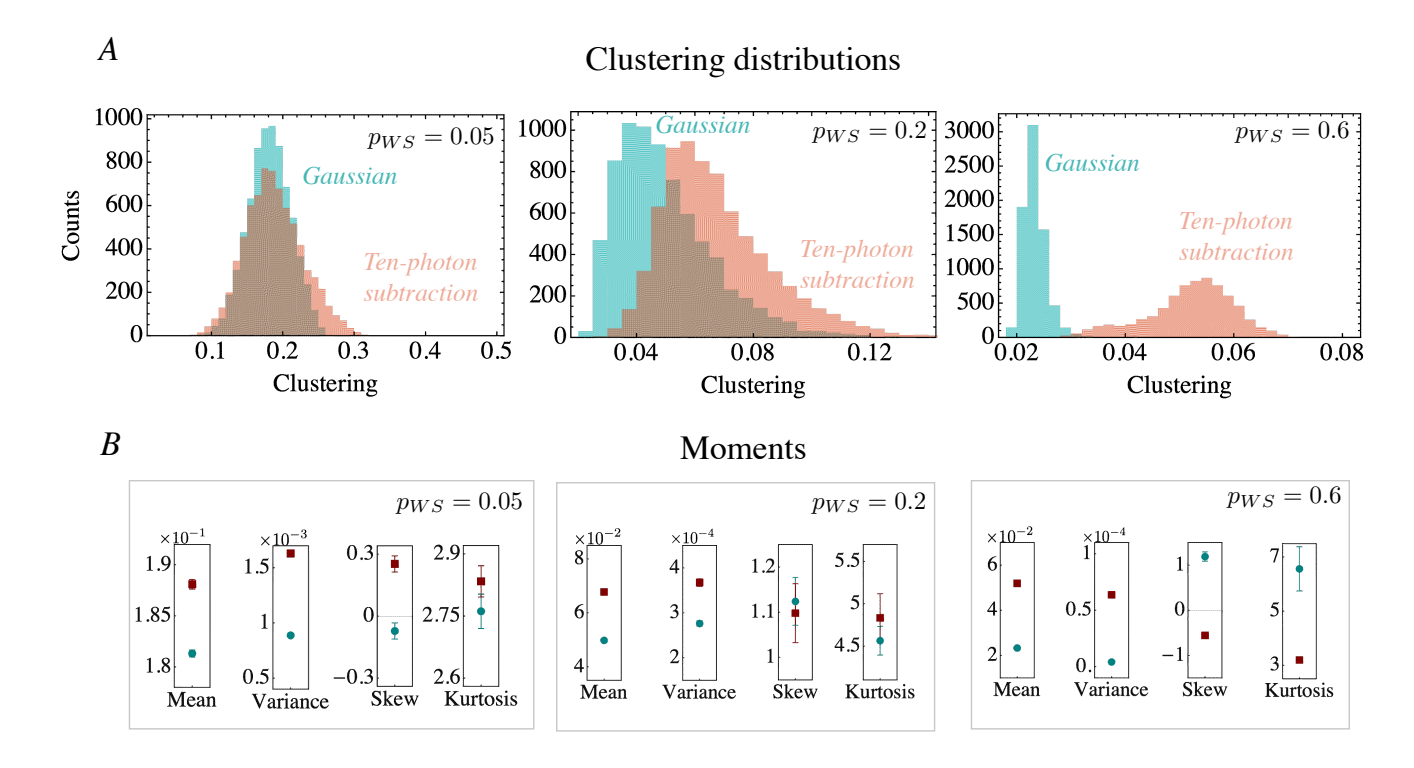


FIG. 10. Histograms (A) and moments (B) for the clustering distributions for the same networks as Fig. 9. Colors indicate degree data prior to (cyan, dots) and after (red, squares) the subtraction of ten photons in the node with the highest connectivity. Photon subtraction shifts and widens the distribution, as shown by the histograms and quantified by the mean and variance. The higher moments and histograms indicate that the finer structure of these distributions depend strongly on the value of p_{WS} .

in smaller values of kurtosis in Fig. 11(B). These moments, nevertheless, show a profound change in the variance due to photon subtraction, which implies an overall widening of the distribution. Figure 11(A) shows this feature, as now a larger fraction of the distribution grows to higher values of the degree. Hence, for m=2 we can conclude that photon subtraction predominantly affects the bulk of the distribution, which is qualitatively similar to what we saw for WS distributions.

In Fig. 12 we observe that for m=1 the clustering coefficients in these networks can be increased up to Cl=0.8, though only for a small fraction of nodes. In other words, photon subtraction, again, predominantly affects the tails of the distribution for m=1 (which is confirmed by the moment analysis in Panel B of Fig. 12). Therefore random tree networks (i.e., BA with m=1) globally seem to be the most resilient networks to local photon subtraction operations, even though photon subtraction in nodes with few links can cause profound local changes in the correlations. For m=2 we again see a larger overall impact of photon subtraction, leading to more significant changes to the bulk of the distribution. This, too, is in line with the degree statistics.

These results suggest that the environment of the subtracted node in the imprinted network plays an important role in how the emergent network reacts to photon subtraction. To unravel this interplay between the imprinted structure and the emergent network, we will investigate the behaviour of nodes depending on their distance (in the imprinted network) to the node of photon subtraction.

V. IMPRINTED STRUCTURE GUIDES NON-GAUSSIAN EFFECTS

A. Distance-induced structure

In Sec. IV, we showed that photon subtraction induces additional structure in the emergent network. Here, we take the first step toward understanding how the emergent structure in photon-number correlations is influenced by the imprinted structure. We break up the statistics according to the imprinted distance between the node in which the photons were subtracted and the nodes under consideration. This distance between nodes is here understood to be the number of connections in the shortest path that connects the nodes in the imprinted structure.

In Sec. IV A we emphasised that the quantity $\langle \hat{n}_i \hat{n}_j \rangle - \langle \hat{n}_i \rangle \langle \hat{n}_j \rangle$ is only altered by photon subtraction when nodes i and j are both in the vicinity of the point of pho-

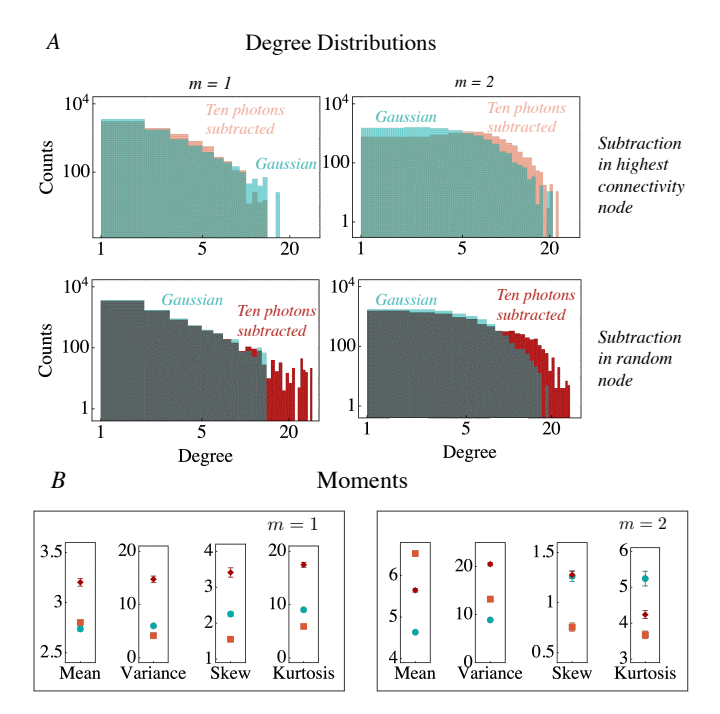


FIG. 11. Logarithmically-scaled histograms (A) and moments (B) for the degree distributions of the emergent correlation network obtained from a BA imprinted structure for networks generated with m=1,2. Colors indicate degree data prior to (cyan, dots) and after the subtraction of ten photons in the node with the highest connectivity (light red squares), or in a randomly chosen (dark red diamonds) node. These histograms were each obtained by combining 100 random realizations of a 100-node network. Photon subtraction mainly affects the tails of the distribution as seen in the histograms and reflected in the variance and kurtosis. The emergent networks for m=1 imprinted structures show power-law behaviour, which is reflected by high values of the kurtosis.

ton subtraction. When at least one of the vertices lies beyond, the features of its emergent correlations are only impacted via the denominator in Eq. (6). For the degree statistics, this means that nodes at distances zero (point of subtraction), one (nearest neighbours), and two (next-to-nearest neighbours) are very differently affected by photon subtraction than the remaining nodes. This motivates the choice to separate the nodes into four groups: the nodes where the photons are subtracted (distance θ); their nearest neighbors (distance θ); and all the remaining nodes (distance θ) or more).

As an example of such a distance analysis, we consider in Fig. 13 four histograms corresponding to our four chosen groups of nodes. A complementary quantitative view can be obtained by studying the moments of these distance-resolved histograms, as shown in the moments of the degree distribution in Fig. 14 for imprinted WS structures and in Fig. 15 for imprinted BA network. A completely analogous analysis can be carried out for the clustering coefficients.

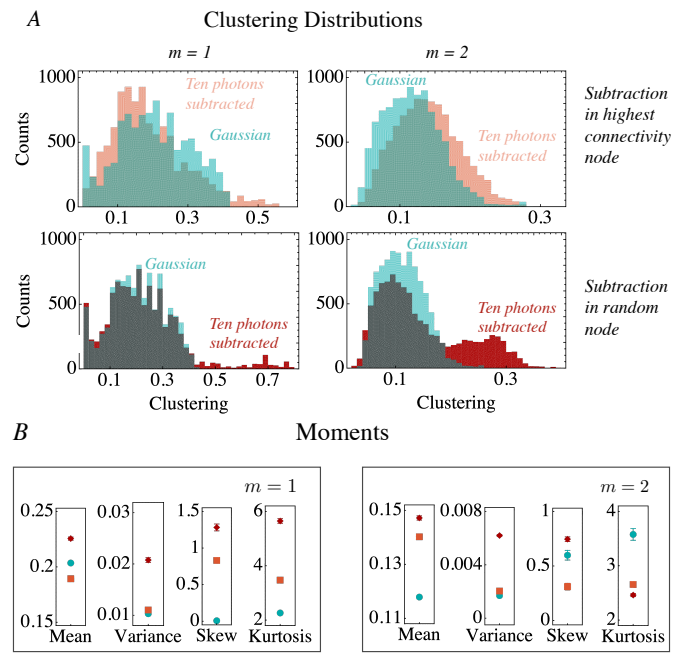


FIG. 12. Histograms (A) and moments (B) for the clustering distributions of the same networks as Fig. 11, and the same color coding. Photon subtractions increase the tails of the distributions. Photon subtraction in a random node can create high clustering coefficients for a reasonably small number of modes.

The moments in Figs. 14 and 15 provide a range of important insights. First, we find that degree distribution of nodes that lie beyond the next-nearest neighbors ($\geqslant 3$) are generally unaltered by photon subtraction. A notable exception is found for the imprinted BA network with photon subtraction in a random node, where the higher moments, i.e., skewness and kurtosis, for these nodes are influenced. This is consistent with the idea that, for an imprinted BA network with photon subtraction in a random node, the non-Gaussian effects are confined to a smaller number of nodes, which in turn change more drastically.

As a second observation, we find that the distance-dependent effects in the skewness and kurtosis depend strongly on the specific network-type and chosen parameters, in contrast to the mean and variance. This implies that photon subtraction induces some general effects on the bulk of degree distributions (as comprised by the first two moments), while the effect on the finer structure (as comprised by the higher moments) of the degree distributions depends more strongly on the precise topology of the imprinted networks.

As an important general effect, we find that both for the nodes in which photons are subtracted (θ) and their next-nearest neighbors (2) the mean and variance of the degree distribution always increase. The behaviour of the nearest neighbors (1) is less systematic. For imprinted BA networks with photon subtraction in a random ver-

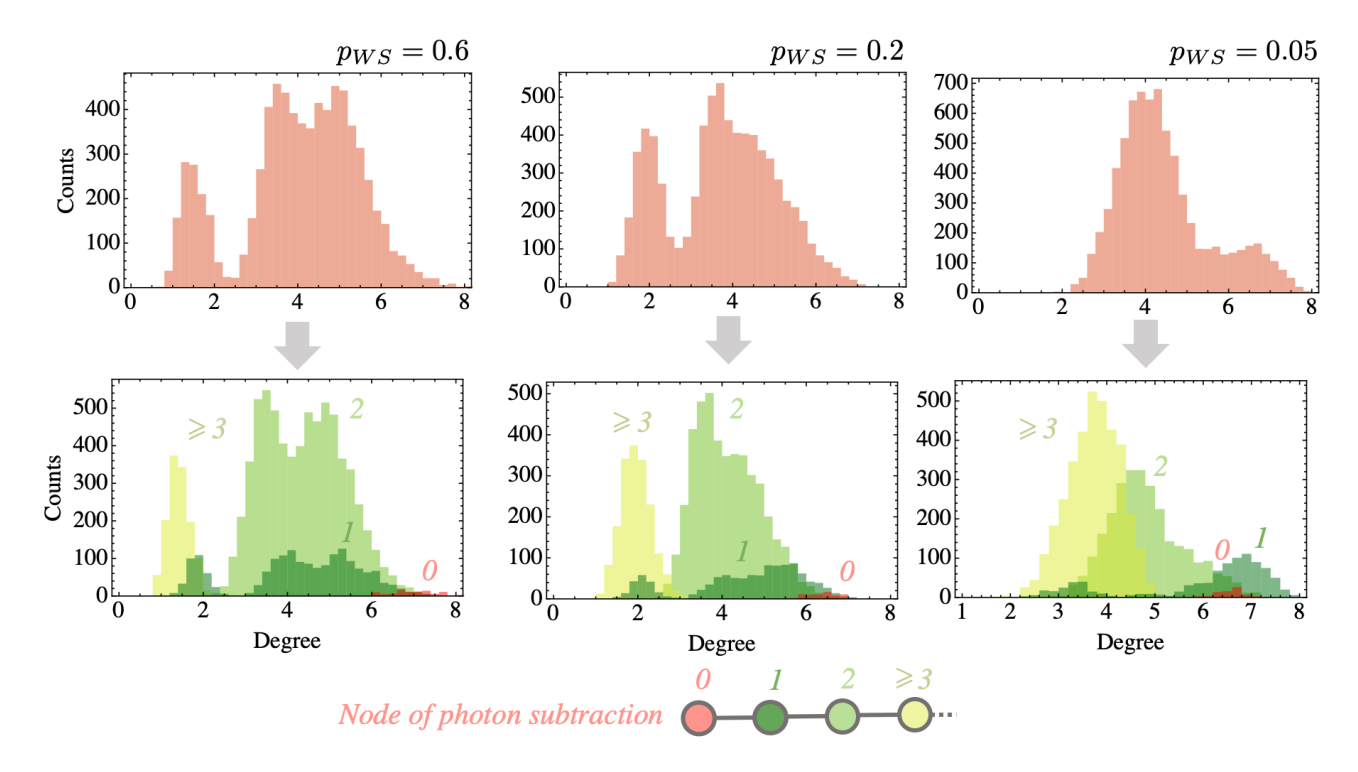


FIG. 13. Degree distribution of the emergent network of imprinted WS networks after the subtraction of ten photons, using the same data as Fig. 9. Complete histograms (top) were each obtained by combining all the nodes of 74 random realizations of a 100-node network (see also Fig. 9). Distance-resolved histograms (bottom) are obtained by grouping nodes based on their network distance (in the imprinted network) to the node of photon subtraction. Network distance is indicated by color code and labeled by a number (zero being the node of subtraction). Photon subtraction shifts the degree distribution to higher values for the nodes of photon subtraction (distance θ) and those at distance 2. At distance 3 and beyond, the effects are negligible. At distance 1 the distribution is affected in a non-trivial way depending on $p_{\rm WS}$. The value of $p_{\rm WS}$ also influences the relative importance of distance-induced features, e.g., for $p_{\rm WS} = 0.05$ we find a larger fraction of nodes at distance 3 or beyond.

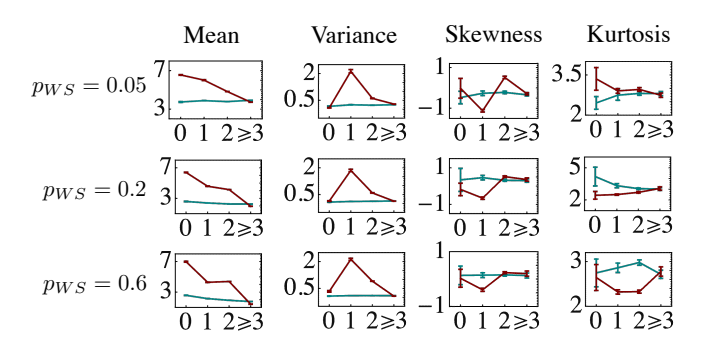


FIG. 14. Distance-resolved moments for the degree statistics in the emergent photon-number correlation network, resulting from imprinted WS networks with rewiring probabilities $p_{\rm WS}=0.05,~p_{\rm WS}=0.2,~{\rm and}~p_{\rm WS}=0.6.$ Gaussian states (cyan) and ten-photon subtracted states (red). Photon subtraction mean and variance are affected in the same way for all networks, showing that photon subtraction has the global tendency of increasing the degree and widening the distribution of nodes up to distance 2. The effect on higher moments depends on the value of $p_{\rm WS}$, showing that photon subtraction also affects the fine structure of the degree distribution in a more subtle way that depends on the network topology. At distance 3 and beyond we see no effect.

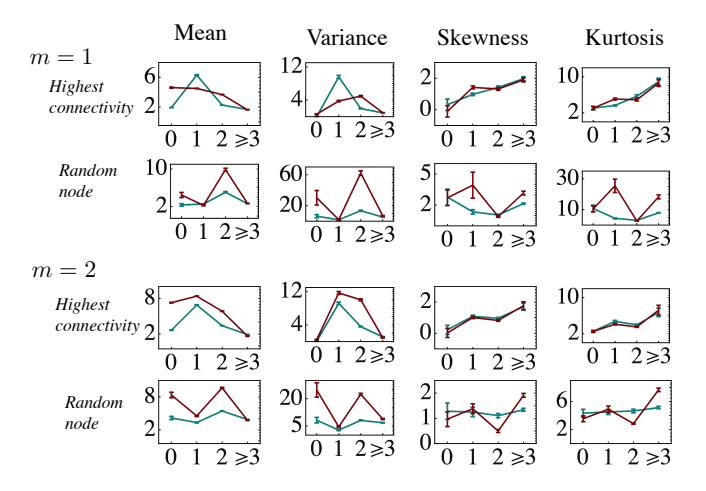


FIG. 15. Distance-resolved moments for the degree statistics in the emergent photon-number correlation network, resulting from imprinted BA networks with parameters m=1 and m=2. Gaussian states (cyan) and ten-photon subtracted states (red). The same observations hold as for the WS networks in Fig. 14, except for the distance 1 nodes in imprinted structures with m=1. The latter is explained in detail in Sec. VB.

tex, the mean and variance are essentially unaltered for the nearest neighbors. In contrast, for imprinted WS networks, and the m=2 BA network with photon subtraction in the node with highest connectivity, the mean and variance increase for these nodes. For the imprinted BA network with m=1 and photon subtraction in the node with highest connectivity, we find that the mean and variance decrease after photon subtraction. Hence, there must be other features in the topology of the imprinted network that influence the degree distribution of the nearest neighbors. These features will be laid out in the following subsection.

B. Nearest neighbors (1) sub-networks

In Fig. 16 we show that the effect on the degree of a nearest-neighbor node in the emergent correlation network is influenced by the number of other nearest neighbors it is connected to in the imprinted networks. This highlights the importance of the topology of the distance-1 sub-network, as compared to the total imprinted network. Quantitatively, this connectivity can be obtained by analyzing the nearest-neighbor sub-network, as highlighted in Fig. 17. When we analyze all the nearestneighbor sub-networks of our simulated WS networks, we obtain the result in Fig. 16. The bottom row of figures clearly shows that the degrees (in the emergent network) of nearest neighbors are more strongly affected by photon subtraction when these nodes have a higher number of connections to other nearest neighbors. Thus, the different shapes of the nearest neighbor distributions (1), for different values of the rewiring probability p_{WS} , can be fully understood from the nearest neighbor sub-network in the imprinted structure.

We note that photon subtraction shifts the histograms which group nearest-neighbor nodes according to their connectivity in the distance-1 sub-network to higher mean values for higher connectivity. However, for nodes that are not connected to other nearest neighbors, we witness a slight decrease in the average degree due to photon subtraction.

For $p_{\rm WS}=0.6$ in Fig. 17, we observe a significant fraction of nearest neighbors that are not connected to any other nearest neighbors. This provides a sharp contrast with the case for $p_{\rm WS}=0.05$, where we observe that networks tend to form clusters, such that nearest neighbors are more likely to be connected to each other. From Fig. 16, we can understand how these features of the imprinted structure have a direct effect on the statistical features of the emergent network.

Similar analyses have been carried out for the nearest neighbor networks of all simulated classes of networks, leading to the same results. A particularly striking case is the BA network with m=1: because these networks are tree-like, nearest neighbors are never connected to one another. This explains why in Fig. 15, for m=1, the means for nearest neighbors (1) are reduced by photon

subtraction. Moreover, we can now explain why the contribution of the nearest-neighbor sub-network for photon subtraction from the highest degree node for BA with m=2 is more important than in the case of subtraction from a random node. In this latter case it is more likely to select one of the isolated nodes with a surrounding nearest-neighbor sub-network also characterized by low connectivity. However, the analysis is not sufficient to explain why the next-nearest neighbors (2) are so strongly affected by photon subtraction from a random node in the BA network with m=2.

VI. SUMMARY, DISCUSSION, AND OUTLOOK

In summary, we have addressed the question of how emergent complexity arises from imprinted complexity in continuous variable (CV) quantum networks. In particular, we have addressed the question of how localized non-Gaussian features, a key feature of CV quantum technologies and quantum networks such as a future quantum internet, spread through emergent network correlations. Specifically, we used tools from complex network theory to analyze emergent networks of photon-number correlations that manifest in CV cluster states. These cluster states were initially taken as Gaussian states, constructed by applying an imprinted network of entangling C_Z gates to a series of squeezed vacuum modes; non-Gaussian states were then created via photon subtraction. We focused on the particular case in which these imprinted networks of quantum gates were chosen to have a complex network structure, implementing either a Watts-Strogatz (WS) or Barabási-Albert (BA) model.

For Gaussian states that were created by imprinting WS networks, we found that increased probability of rewiring (and thus more randomness) in the imprinted networks decreases the typical degree and clustering coefficient in the emergent correlation network. When BA structures were imprinted, we found that emergent correlation networks inherit heavy tails with a structure that is strongly influenced by the number m of connections added with every node in the BA preferential attachment process. For tree networks (m=1), the emergent networks was found to inherit a power-law tail in its degree statistics. In contrast, this power-law behavior was not observed for m=2.

We rendered the states non-Gaussian by subtracting ten photons in a specific node of the system. The short distance between the different nodes in the network guaranteed that the effect of photon subtraction spread far throughout the state. We showed that network theory methods are well-suited to characterize the resulting non-Gaussian states, as photon subtraction was found to profoundly change the structure of the emergent networks (see Fig. 5 for an example). We quantified this effect by comparing the distributions of the degrees and clustering coefficients before and after photon subtraction. Generally, we found that photon subtraction increased

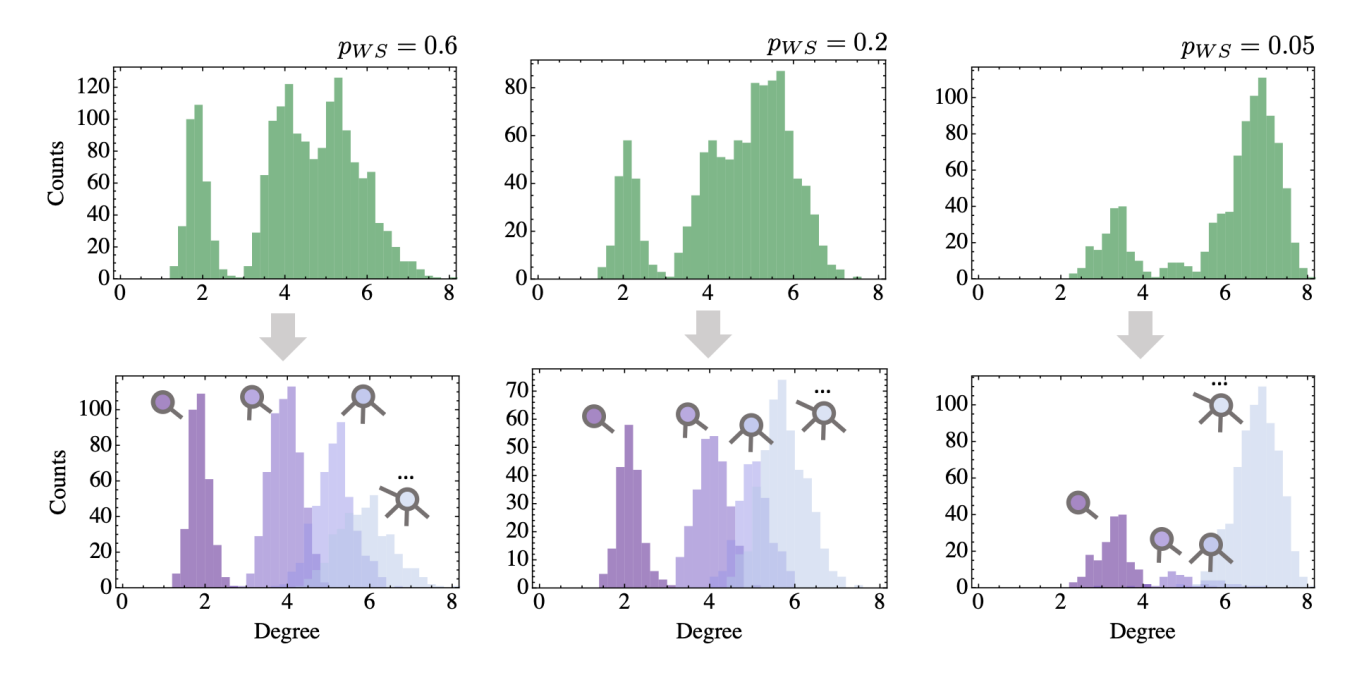


FIG. 16. Nearest-neighbor (1) degree distribution of the emergent network after the subtraction of ten photons, using the same data as Fig. 13. Top row: complete nearest-neighbor histograms. Bottom row: histograms obtained by grouping nearest-neighbor nodes based on the number of other nearest-neighbor nodes they are connected to in the nearest-neighbour sub-network. The connectivity in the nearest-neighbor sub-network is highlighted by the nodes represented next to the histogram. Nearest neighbors of the node of photon subtraction are more strongly affected by the non-Gaussian operation when they are connected to other nearest neighbors. Nodes that are not connected to any other nearest neighbors (darkest purple) are shifted to lower degrees as compared to the Gaussian distributions in Fig. 9.

the typical degree and clustering coefficient, as seen from the mean, and increased the spread of these quantities as characterized by a growing variance. However, we also observed that the higher moments, and thus the finer structure in the tails of the distributions, depended more strongly on the network types and chosen parameters. For BA imprinted networks, we found a strong variation in behaviour of the emergent correlation network depending on whether the photons are subtracted from a hub or a random node. This highlights the importance of the local network topology in the vicinity of the node of photon-subtraction.

We proceeded to dissect the structure of the emergent correlation networks, based on the features of the imprinted network. As a first step, in Sec. VA, we filtered nodes in the emergent network based on their distance to the node of photon subtraction in the imprinted network. Generally, we found that the photon subtraction increases the variance and the mean in the nodes of photon subtraction (distance θ), while for next-nearest neighbors (distance 2) the first two moments of nodes that were further removed (distance ≥ 3) remained unaffected. However, the nearest neighbors (distance 1) in imprinted tree networks defied this global trend. In Sec. VB we showed this is due to the particular structure of the nearest-neighbor sub-networks that are extracted from the imprinted network. When we further filtered the nodes at distance 1 based on their connectivity to

other nodes at distance 1, we found that higher connectivity led to a stronger increase in the typical degree due to photon subtraction. In other words, nearest-neighbor nodes were more strongly affected by photon subtraction if they were connected to many other nearest-neighbour nodes. In a tree network, nearest neighbours can never be connected to other nearest neighbors, which slightly decreased the average degree in the correlation network for the nodes at distance 1. The distance-resolved moment analysis furthermore showed that the fine structure in the tails of the distributions, as captured by higher moments, does depend strongly on the network topology.

The structural features we uncovered help us understand that the bulk features of emergent correlation networks of imprinted tree structures are only slightly impacted by photon subtraction. The effects that do manifest are mainly observed in the tails of the distribution, as seen in the moment analysis. difference between subtraction in a random vs. highly connected node is particularly interesting when interpreted in the light of the network structure. Photon subtraction is a finite resource to enhance correlations in the system. On the one hand, in a node that is correlated to only a small number of other nodes it significantly increases correlations between this small set of nodes, thus causing larger values to appear in the tails. On the other hand, when a photon is subtracted in a hub with very high number of nodes

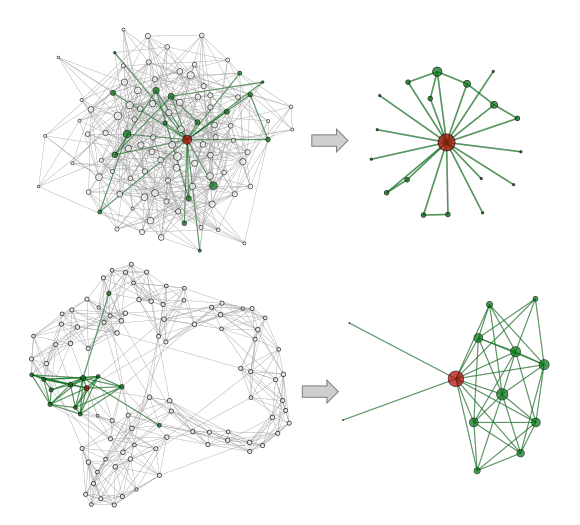


FIG. 17. WS networks obtained from rewiring a regular 1D network, where every node is connected to its k=5 nearest neighbors, with rewiring probability $p_{\rm WS}=0.6$ (top) and $p_{\rm WS}=0.05$ (bottom). The subtraction node is highlighted in red, whereas the nearest neighbor sub-network is shown in green. We thus illustrate that the value of $p_{\rm WS}$ strongly influences the typical structure of the nearest-neighbor network, which in turn strongly influences the relative importance of the different histograms in the bottom row of Fig. 16.

correlated to it, the increase in correlations is spread out.

This work represents a first test of complex network structures in the CV quantum regime under the applications of necessary non-Gaussian operations. We believe this investigation can be fruitful for making decisions about the structure of future quantum technologies on a large scale.

Moreover, complex network methods have proven useful for the theoretical investigation of such classes of states. Indeed, the characterization of highly multimode non-Gaussian states is generally an arduous task, where standard tools of CV quantum optics fall short. Typical experimental methods such as homodyne tomography lack the necessary scaling properties to study these systems, and theoretical constructs such as Wigner functions become hard to handle. To overcome this problem, one may look for global properties, e.g., Wigner negativity of the full multimode states [20]. Such global features have the disadvantage that they gloss over the local or neighborhood structures of the state, which are essential in multi-partite quantum platforms. Our results show that network theory offers effective statistical tools for studying these states. At present, we are unaware of any other method that allows us to describe the physical features that we deduced for these large non-Gaussian states. They offer us a road map for more detailed bottom-up studies of particular features such as the role of connections in the nearest-neighbor sub-network.

ACKNOWLEDGMENTS

This work was supported by the European Research Council under the Consolidator Grant COQCOoN (Grant No. 820079). This work was also performed in part with support by the U.S. National Science Foundation under grants CCF-1839232, OAC-1740130, PHY-1806372, and PHY-1748958; and in conjunction with the QSUM program, which is supported by the Engineering and Physical Sciences Research Council grant EP/P01058X/1. We thank the Complex Quantum Systems group at Laboratoire Kastler Brossel (and in particular D. Delande) for access to their computational facilities.

The software used to generate the complex networks in the Article is available on [96]

Appendix A: Simulating cluster states and the evaluation of photon-number correlations

1. Perfect matching

To execute the simulations presented in this article, we generated random complex networks using the "python-inetwork" library. From these randomly generated networks, we extracted the adjacency matrix \mathcal{A} to generate the cluster state covariance matrices, as described in Eq. (4). After generating the covariance matrix V of a Gaussian network state, we used it to evaluate the photon-number correlations $[\mathbb{C}]_{ij}$ of Eq. (6) for the photon-subtracted states in Eq. (5).

The main technique used to evaluate these correlations relies on the properties of Gaussian quantum states. We previously used this method to fully characterize single-photon subtracted states in [16]. We illustrate this method by highlighting the evaluation of the element $\langle \hat{n}_i \hat{n}_j \rangle$ in Eq. (6). For a photon-subtracted state we find

$$\langle \hat{n}_i \hat{n}_j \rangle = \frac{\operatorname{tr}[\hat{a}_{S_n}^{\dagger} \dots \hat{a}_{S_1}^{\dagger} \hat{a}_i^{\dagger} \hat{a}_j^{\dagger} \hat{a}_j \hat{a}_i \hat{a}_{S_1} \dots \hat{a}_{S_n} \rho]}{\operatorname{tr}[\hat{a}_{S_n}^{\dagger} \dots \hat{a}_{S_1}^{\dagger} \hat{a}_{S_1} \dots \hat{a}_{S_n} \rho]}, \quad (A1)$$

where ρ denotes the density matrix of the Gaussian network state and $i \neq j$. We then use a general property for Gaussian states, that allows us to express

$$\operatorname{tr}[\hat{a}_{S_{n}}^{\dagger} \dots \hat{a}_{S_{1}}^{\dagger} \hat{a}_{i}^{\dagger} \hat{a}_{j}^{\dagger} \hat{a}_{j} \hat{a}_{i} \hat{a}_{S_{1}} \dots \hat{a}_{S_{n}} \rho]$$

$$= \sum_{\mathcal{P}} \prod_{\{p_{1}, p_{2}\} \in \mathcal{P}} \operatorname{tr}[\hat{a}_{p_{1}}^{\#} \hat{a}_{p_{2}}^{\#} \rho],$$
(A2)

where we introduce the label \mathcal{P} to denote a "perfect matching." A perfect matching means any way of dividing a set up into pairs, while maintaining the order. When we consider, for example the set $\{1,2,3,4\}$, one possible perfect matching would be $\{\{1,3\},\{2,4\}\}$. In this example, the notation $\{p_1,p_2\} \in \mathcal{P}$ refers to $\{1,3\}$ and $\{2,4\}$. In Eq. (A2), these perfect matchings are

used to split the set of creation and annihilation operators, $\hat{a}_{S_n}^{\dagger} \dots \hat{a}_{S_1}^{\dagger} \hat{a}_i^{\dagger} \hat{a}_j^{\dagger} \hat{a}_j \hat{a}_i \hat{a}_{S_1} \dots \hat{a}_{S_n}$, in pairs: In total, we have 2n+4 creation and annihilation operators, which we can associate with a set of indices $\{1,\dots,2n+4\}$. The sum over \mathcal{P} runs over all possible perfect matchings of this index set. For every given perfect matching \mathcal{P} , we then multiply all the quantities $\operatorname{tr}[\hat{a}_{p_1}^{\#}\hat{a}_{p_2}^{\#}\rho]$ for the different paired indices $\{p_1,p_2\}\in\mathcal{P}$. The quantities p_1 and p_2 are indices in the index set, and the quantity $\hat{a}_{p_j}^{\#}$ denotes the creation or annihilation operator that occurs at the p_j th position in the product $\hat{a}_{S_n}^{\dagger}\dots\hat{a}_{S_1}^{\dagger}\hat{a}_i^{\dagger}\hat{a}_j\hat{a}_i\hat{a}_i\hat{a}_{S_1}\dots\hat{a}_{S_n}$. Let us list some examples: $\operatorname{tr}[\hat{a}_1^{\#}\hat{a}_2^{\#}\rho] = \operatorname{tr}[\hat{a}_{S_1}^{\dagger}\hat{a}_j^{\dagger}\hat{a}_j\hat{a}_i\hat{a}_{S_1}\rho]$, $\operatorname{tr}[\hat{a}_2^{\#}\hat{a}_{n+3}^{\#}\rho] = \operatorname{tr}[\hat{a}_{S_2}^{\dagger}\hat{a}_j\rho]$, and $\operatorname{tr}[\hat{a}_1^{\#}\hat{a}_{n+5}^{\#}\rho] = \operatorname{tr}[\hat{a}_{S_1}^{\dagger}\hat{a}_{S_1}\rho]$.

What remains is now to evaluate the quantities $\operatorname{tr}[\hat{a}_{p_1}^{\#}\hat{a}_{p_2}^{\#}\rho]$, and this can be done directly via the covariance matrix V, by expressing the creation and annihilation operators in terms of quadrature operators (see also [16, 97] for more details). We find the following identities:

$$\operatorname{tr}[\hat{a}_{j}^{\dagger}\hat{a}_{k}^{\dagger}\rho] = \frac{1}{4}[V_{jk} - V_{j+N,k+N} - i(V_{j,k+N} + V_{j+N,k})], \tag{A3}$$

$$\operatorname{tr}[\hat{a}_{j}\hat{a}_{k}\rho] = \frac{1}{4}[V_{jk} - V_{j+N,k+N} + i(V_{j,k+N} + V_{j+N,k})], \tag{A4}$$

$$\operatorname{tr}[\hat{a}_{j}^{\dagger}\hat{a}_{k}\rho] = \frac{1}{4}[V_{jk} + V_{j+N,k+N} + i(V_{j,k+N} - V_{j+N,k}) - 2\delta_{jk}]. \tag{A5}$$

These identities are expressed in the mode basis that corresponds to the nodes of the network state.

Using Eqs. (4) and (A3)-(A5), we can calculate the weighted adjacency matrix of the emergent network, \mathbb{A}_{ij} . In principle, it is possible to calculate \mathbb{A}_{ij} for both the cluster state as well as the photon-subtracted state. However, as we will show, it is exponentially difficult to write a closed-form expression for \mathbb{A}_{ij} in the photon-subtracted state. Below, we will first calculate \mathbb{A}_{ij} in the cluster state. Then we discuss the photon-subtracted case.

2. Gaussian state

Since the cluster state ρ is Gaussian, one can evaluate the connected correlation $c_{ij} \equiv \operatorname{tr}[\hat{n}_i \hat{n}_j \rho] - \operatorname{tr}[\hat{n}_i \rho] \operatorname{tr}[\hat{n}_j \rho]$ by applying Eq. (A2). Only two terms remain, giving

$$c_{ij} = \operatorname{tr}[\hat{a}_i^{\dagger} \hat{a}_j \rho] \operatorname{tr}[\hat{a}_i \hat{a}_j^{\dagger} \rho] + \operatorname{tr}[\hat{a}_i^{\dagger} \hat{a}_j^{\dagger} \rho] \operatorname{tr}[\hat{a}_i \hat{a}_j \rho].$$
 (A6)

Each term on the right hand side of Eq. (A6) can be evaluated using Eqs. (4) and (A3)-(A5).

For $i \neq j$, we have

$$\operatorname{tr}[\hat{a}_{i}^{\dagger}\hat{a}_{j}\rho] = s(\mathcal{A}^{2})_{ij}/4,$$

$$\operatorname{tr}[\hat{a}_{i}\hat{a}_{j}^{\dagger}\rho] = s(\mathcal{A}^{2})_{ij}/4,$$

$$\operatorname{tr}[\hat{a}_{i}^{\dagger}\hat{a}_{j}^{\dagger}\rho] = -(s(\mathcal{A}^{2})_{ij} - 2is\mathcal{A}_{ij})/4,$$

$$\operatorname{tr}[\hat{a}_{i}\hat{a}_{j}\rho] = -(s(\mathcal{A}^{2})_{ij} + 2is\mathcal{A}_{ij})/4.$$
(A7)

Therefore

$$c_{ij} = \frac{s^2}{8} \left((A^2)_{ij}^2 + 2A_{ij} \right)$$
 (A8)

where we used that $(A_{ij})^2 = A_{ij}$. For i = j, we have

$$\operatorname{tr}[\hat{a}_{i}^{\dagger}\hat{a}_{i}\rho] = (s + 1/s + s\mathcal{D}_{i} - 2)/4,$$

$$\operatorname{tr}[\hat{a}_{i}\hat{a}_{i}^{\dagger}\rho] = (s + 1/s + s\mathcal{D}_{i} + 2)/4,$$

$$\operatorname{tr}[\hat{a}_{i}^{\dagger}\hat{a}_{i}^{\dagger}\rho] = (s - 1/s - s\mathcal{D}_{i})/4,$$

$$\operatorname{tr}[\hat{a}_{i}\hat{a}_{i}\rho] = (s - 1/s - s\mathcal{D}_{i})/4,$$
(A9)

where we used that $A_{ii} = 0$ and $(A^2)_{ii} = D_i$. Therefore

$$c_{ii} = \frac{1}{8} \left(s^2 + \frac{1}{s^2} + s^2 (\mathcal{D}_i)^2 + 2\mathcal{D}_i - 2 \right).$$
 (A10)

One obtains Eq. (10) in the main text from Eqs. (A8) and (A10), where c_{ii} is denoted in the main text as $\mathfrak{N}(s, \mathfrak{D}_i)$.

3. Photon-subtracted states

For photon-subtracted states, the correlations quickly become hard to evaluate. At the basis of this complexity lies the appearance of perfect matchings in Eq. (A2). Finding all possible perfect matchings is a computationally hard problem that belongs to the complexity class #P. It is also the problem which lies at the basis of the hardness of Gaussian Boson Sampling. Hence, when the number of subtracted photons grows, correlation functions quickly become practically impossible to evaluate.

Generally speaking, the best algorithms for evaluating Eq. (A2) use recursive techniques. In our work, we greatly simplify this computational problem by subtracting all the photons in the same mode, i.e., $S_1 = \cdots = S_n = S$. In this case, expression (A1) for $\langle \hat{n}_i \hat{n}_j \rangle$ only contains creation and annihilation operators in three different modes. This greatly limits the different possible factors $\text{tr}[\hat{a}_{p_1}^{\#}\hat{a}_{p_2}^{\#}\rho]$ that can appear in Eq. (A2). Many different partitions will lead to equivalent contributions. The problem thus reduces to that of identifying all the different classes of partitions, evaluating the contribution, and counting the multiplicity.

Once we subtract more than three photons, the total number of different classes of terms remains fixed. We evaluated these by hand and counted a total of 43 classes, each appearing with a certain multiplicity. The

correlation networks are then calculated by evaluating the contribution by multiplying relevant quantities given by Eqs. (A3) - (A5) for each of these 43 classes. Then we multiply each contribution with the right multiplicity, which depends on the number of subtractions and can be calculated through combinatorics. The quantities $\langle \hat{n}_i \rangle$ are evaluated using the same method. For more details, we refer to the code that was used to carry out the simulations [96].

Appendix B: Correlations unaffected by photon subtraction

In this section of the appendix, we prove a general result for correlations in n-photon subtracted states: photon subtraction can only change the covariance between observables, if both observables are initially correlated to the mode in which the photons are subtracted.

Assume that we subtract n photons from Gaussian state ρ in a mode with label S and associated annihilation operator \hat{a}_S . We denote the algebra of observables $\mathcal{A}_{\text{near}}$ as those observables which are "near to S" in the sense that $\mathcal{A}_{\text{near}}$ is generated by observables \hat{a}_k and \hat{a}_k^{\dagger} for which either $\text{tr}[[\rho]\hat{a}_k^{\dagger}\hat{a}_S] \neq 0$ or $\text{tr}[[\rho]\hat{a}_k\hat{a}_S] \neq 0$. Following Eqs. (A3)-(A5) we can equivalently define $\mathcal{A}_{\text{near}}$ as the algebra of observables restricted to the modes with labels k for which the matrix

$$\begin{pmatrix} V_{Sk} & V_{S\,k+N} \\ V_{S+N\,k} & V_{S+N\,k+N} \end{pmatrix} \neq \begin{pmatrix} 0 & 0 \\ 0 & 0 \end{pmatrix}$$
 (B1)

We then define \mathcal{A}_{far} as the complement of $\mathcal{A}_{\text{near}}$ in the sense that $\mathcal{A}_{\text{near}} \otimes \mathcal{A}_{\text{far}} = \mathcal{A}$, where \mathcal{A} is the full algebra of observables on the N-mode Fock space that describes the entire system.

Theorem B.1. For any observable $\hat{X} \in \mathcal{A}_{near}$ and another arbitrary observable $\hat{Y} \in \mathcal{A}_{far}$, it holds that

$$\langle \hat{X}\hat{Y}\rangle - \langle \hat{X}\rangle\langle \hat{Y}\rangle = \text{tr}[\hat{X}\hat{Y}\rho] - \text{tr}[\hat{X}\rho]\text{tr}[\hat{Y}\rho],$$
 (B2)

where $\langle ... \rangle$ denotes the expectation value in the n-photon subtracted state and $tr[...\rho]$ is the expectation value in the initial Gaussian state.

Proof. We first of all use that every observable $\hat{X} \in \mathcal{A}_{near}$ can be arbitrarily well approximated by a polynomial in creation and annihilation operators in \mathcal{A}_{near} . This implies that

$$\hat{X} = \sum_{j=0}^{\infty} \sum_{k} c_{j,k} \hat{a}_{1,k}^{\#} \dots \hat{a}_{j,k}^{\#},$$
 (B3)

where $\hat{a}_{1,k}^{\#}$ can either be a creation or an annihilation operator. The sum over k takes into account that there are many possible products of creation and annihilation operators, also known as Wick monomials, of length i.

And similarly for \hat{Y} we find

$$\hat{Y} = \sum_{j=0}^{\infty} \sum_{k} c_{j,k} \hat{b}_{1,k}^{\#} \dots \hat{b}_{j,k}^{\#},$$
 (B4)

To highlight that the creation and annihilation operators that build \hat{X} and \hat{Y} have different supports, we have noted the tre creation and annihilation operators for $\mathcal{A}_{\mathrm{far}}$ as $\{b_{j,k}^{\#}\}$.

The fact that any observable can be written as a series

The fact that any observable can be written as a series expansion of creation and annihilation operators implies that our theorem can be proven by proving that

$$\langle \hat{a}_{1}^{\#} \dots \hat{a}_{j}^{\#} \hat{b}_{1}^{\#} \dots \hat{b}_{j'}^{\#} \rangle - \langle \hat{a}_{1}^{\#} \dots \hat{a}_{j}^{\#} \rangle \langle \hat{b}_{1}^{\#} \dots \hat{b}_{j'}^{\#} \rangle$$

$$= \operatorname{tr}[\hat{a}_{1}^{\#} \dots \hat{a}_{j}^{\#} \hat{b}_{1}^{\#} \dots \hat{b}_{j'}^{\#} \rho] - \operatorname{tr}[\hat{a}_{1}^{\#} \dots \hat{a}_{j}^{\#} \rho] \operatorname{tr}[\hat{b}_{1}^{\#} \dots \hat{b}_{j'}^{\#} \rho],$$
(B5)

First of all, let us consider the term

$$\langle \hat{b}_1^{\#} \dots \hat{b}_{j'}^{\#} \rangle = \frac{\operatorname{tr}\left[\left(\hat{a}_S^{\dagger}\right)^n \hat{b}_1^{\#} \dots \hat{b}_{j'}^{\#} \left(\hat{a}_S\right)^n \rho\right]}{\operatorname{tr}\left[\left(\hat{a}_S^{\dagger}\right)^n \left(\hat{a}_S\right)^n \rho\right]}$$
(B6)

Because $\hat{b}_1^{\#}, \dots, \hat{b}_{j'}^{\#} \in \mathcal{A}_{\mathrm{far}}$, we find that $\mathrm{tr}[[\rho]\hat{b}_k^{\dagger}\hat{a}_S] = 0$ and $\mathrm{tr}[[\rho]\hat{b}_k\hat{a}_S] = 0$. An application of Eq.(A2) than shows that

$$\operatorname{tr}\left[\left(\hat{a}_{S}^{\dagger}\right)^{n}\hat{b}_{1}^{\#}\dots\hat{b}_{j'}^{\#}\left(\hat{a}_{S}\right)^{n}\rho\right]$$

$$=\operatorname{tr}\left[\left(\hat{a}_{S}^{\dagger}\right)^{n}\left(\hat{a}_{S}\right)^{n}\rho\right]\operatorname{tr}\left[\hat{b}_{1}^{\#}\dots\hat{b}_{j'}^{\#}\rho\right]$$
(B7)

When we then take into account the denominator in Eq.(B6), we find

$$\langle \hat{b}_{1}^{\#} \dots \hat{b}_{j'}^{\#} \rangle = \text{tr} \left[\hat{b}_{1}^{\#} \dots \hat{b}_{j'}^{\#} \rho \right],$$
 (B8)

it automatically follows that $\langle \hat{Y} \rangle = \text{tr}[\hat{Y}\rho]$.

The expectation value $\langle \hat{a}_1^{\#} \dots \hat{a}_j^{\#} \rangle$ is much more intricate to evaluate since by construction either $\operatorname{tr}[[\rho]\hat{a}_k^{\dagger}\hat{a}_S] \neq 0$ or $\operatorname{tr}[[\rho]\hat{a}_k\hat{a}_S] \neq 0$. We then find

$$\operatorname{tr}\left[\left(\hat{a}_{S}^{\dagger}\right)^{n} \hat{a}_{1}^{\#} \dots \hat{a}_{j}^{\#} \left(\hat{a}_{S}\right)^{n} \rho\right] = \sum_{\mathcal{P}} \prod_{\{p_{1}, p_{2}\} \in \mathcal{P}} \operatorname{tr}\left[\hat{a}_{p_{1}}^{\#} \hat{a}_{p_{2}}^{\#} \rho\right]$$
$$= \operatorname{tr}\left[\left(\hat{a}_{S}^{\dagger}\right)^{n} \left(\hat{a}_{S}\right)^{n} \rho\right] \operatorname{tr}\left[\hat{a}_{1}^{\#} \dots \hat{a}_{j}^{\#} \rho\right] + \operatorname{cross terms}.$$
(B9)

We therefore find that

$$\langle \hat{a}_1^{\#} \dots \hat{a}_j^{\#} \rangle = \operatorname{tr} \left[\hat{a}_1^{\#} \dots \hat{a}_j^{\#} \rho \right] + \Im.$$
 (B10)

The cross terms \mathfrak{I} contain expectation values that combine creation or annihilation operators of the Wick monomial $\hat{a}_1^{\#} \dots \hat{a}_j^{\#}$ with either \hat{a}_S or \hat{a}_S^{\dagger} as obtained from the perfect matching [Eq. (B9)]. For what follows, it is useful to explicitly identify these cross terms as

$$\mathfrak{I} = \langle \hat{a}_1^{\#} \dots \hat{a}_j^{\#} \rangle - \operatorname{tr} \left[\hat{a}_1^{\#} \dots \hat{a}_j^{\#} \rho \right]. \tag{B11}$$

Finally, we can now consider $\langle \hat{a}_1^\# \dots \hat{a}_j^\# \hat{b}_1^\# \dots \hat{b}_{j'}^\# \rangle$ and apply many of the same lines of reasoning. We express

$$\operatorname{tr}\left[\left(\hat{a}_{S}^{\dagger}\right)^{n} \hat{a}_{1}^{\#} \dots \hat{a}_{j}^{\#} \hat{b}_{1}^{\#} \dots \hat{b}_{j'}^{\#} (\hat{a}_{S})^{n} \rho\right]$$

$$= \sum_{\mathcal{P}} \prod_{\{p_{1}, p_{2}\} \in \mathcal{P}} \operatorname{tr}\left[\hat{a}_{p_{1}}^{\#} \hat{a}_{p_{2}}^{\#} \rho\right],$$
(B12)

where $\hat{a}_{p_i}^\#$ can either be a creation/annihilation operator of the type \hat{a} or of the type \hat{b} . A wide variety of terms will appear in the set of perfect matchings [Eq. (B12)]. Generally speaking, we have the terms related to $\hat{a}_1^\# \dots \hat{a}_j^\#$, those related to photon subtraction, i.e., \hat{a}_S or \hat{a}_S^\dagger , and those related to $\hat{b}_1^\# \dots \hat{b}_{j'}^\#$. The crucial element is that $\text{tr}[[\rho]\hat{b}_k^\dagger\hat{a}_S]=0$ and $\text{tr}[[\rho]\hat{b}_k\hat{a}_S]=0$, which implies that any perfect matching that matches a subtraction operator \hat{a}_S or \hat{a}_S^\dagger with a creation or annihilation operator that originates from $\hat{b}_1^\# \dots \hat{b}_{j'}^\#$ vanishes. In other words, the subtraction operators \hat{a}_S or \hat{a}_S^\dagger can be matched only with creation and annihilation operators that live on $\mathcal{A}_{\text{near}}$. This implies that we can rewrite

$$\frac{\operatorname{tr}[\left(\hat{a}_{S}^{\dagger}\right)^{n}\hat{a}_{1}^{\#}\dots\hat{a}_{j}^{\#}\hat{b}_{1}^{\#}\dots\hat{b}_{j'}^{\#}\left(\hat{a}_{S}\right)^{n}\rho]}{\operatorname{tr}\left[\left(\hat{a}_{S}^{\dagger}\right)^{n}\left(\hat{a}_{S}\right)^{n}\rho\right]}$$

$$=\operatorname{tr}[\hat{a}_{1}^{\#}\dots\hat{a}_{j}^{\#}\hat{b}_{1}^{\#}\dots\hat{b}_{j'}^{\#}\rho]$$

$$+\frac{\operatorname{tr}[\hat{b}_{1}^{\#}\dots\hat{b}_{j'}^{\#}\rho]\operatorname{tr}[\left(\hat{a}_{S}^{\dagger}\right)^{n}\hat{a}_{1}^{\#}\dots\hat{a}_{j}^{\#}\left(\hat{a}_{S}\right)^{n}\rho\right]}{\operatorname{tr}\left[\left(\hat{a}_{S}^{\dagger}\right)^{n}\left(\hat{a}_{S}\right)^{n}\rho\right]}$$

$$-\operatorname{tr}[\hat{a}_{1}^{\#}\dots\hat{a}_{j}^{\#}\rho]\operatorname{tr}[\hat{b}_{1}^{\#}\dots\hat{b}_{j'}^{\#}\rho]$$

$$=\operatorname{tr}[\hat{a}_{1}^{\#}\dots\hat{a}_{j}^{\#}\hat{b}_{1}^{\#}\dots\hat{b}_{j'}^{\#}\rho]+\operatorname{tr}[\hat{b}_{1}^{\#}\dots\hat{b}_{j'}^{\#}\rho]\langle\hat{a}_{1}^{\#}\dots\hat{a}_{j}^{\#}\rangle}$$

$$-\operatorname{tr}[\hat{a}_{1}^{\#}\dots\hat{a}_{j}^{\#}\rho]\operatorname{tr}[\hat{b}_{1}^{\#}\dots\hat{b}_{j'}^{\#}\rho].$$
(B13)

where the term $\operatorname{tr}[\hat{a}_1^{\#}\dots\hat{a}_j^{\#}\rho]\operatorname{tr}[\hat{b}_1^{\#}\dots\hat{b}_{j'}^{\#}\rho]$ is subtracted to avoid double counting. We can then use the definition of the cross terms (B11) to write

$$\langle \hat{a}_{1}^{\#} \dots \hat{a}_{j}^{\#} \hat{b}_{1}^{\#} \dots \hat{b}_{j'}^{\#} \rangle = \operatorname{tr}[\hat{a}_{1}^{\#} \dots \hat{a}_{j}^{\#} \hat{b}_{1}^{\#} \dots \hat{b}_{j'}^{\#} \rho] + \operatorname{\mathfrak{T}tr}[\hat{b}_{1}^{\#} \dots \hat{b}_{j'}^{\#} \rho].$$
(B14)

This provides us with the final ingredient we need to complete the proof.

When the results (B8), (B10), and (B14) are combined, we find that all terms proportional to \Im drop out. As such, we find indeed that the identity (B5) holds. Because the identity holds for all possible Wick monomials, it follows that

$$\langle \hat{X}\hat{Y}\rangle - \langle \hat{X}\rangle\langle \hat{Y}\rangle = \operatorname{tr}[\hat{X}\hat{Y}\rho] - \operatorname{tr}[\hat{X}\rho]\operatorname{tr}[\hat{Y}\rho], \quad (B15)$$

for any par of observables $\hat{X} \in \mathcal{A}_{\text{near}}$ and $\hat{Y} \in \mathcal{A}_{\text{far}}$. \square

In full analogy, one can prove a second theorem **Theorem B.2.** For any observables $\hat{X}, \hat{Y} \in \mathcal{A}_{far}$, it holds that

$$\langle \hat{X}\hat{Y}\rangle - \langle \hat{X}\rangle\langle \hat{Y}\rangle = \operatorname{tr}[\hat{X}\hat{Y}\rho] - \operatorname{tr}[\hat{X}\rho]\operatorname{tr}[\hat{Y}\rho], \quad (B16)$$

where $\langle ... \rangle$ denotes the expectation value in the n-photon subtracted state and $tr[...\rho]$ is the expectation value in the initial Gaussian state.

Proof. The proof is fully analogous to Theorem B.1. The only modification it that in the present case the cross terms all vanish, such that $\mathcal{T} = 0$.

Appendix C: Moment analysis

To provide a complementary quantitative grasp on the statistics of the degrees and clustering coefficients of the emergent networks of photon-number correlations as defined in Eq. (6), we analyzed the moments of these distributions. More specifically, we considered the first four non-trivial moments: mean, variance, skew, and kurtosis. For an arbitrary stochastic variable X, these quantities are defined as

$$Mean = \mathbb{E}[X], \tag{C1}$$

Variance =
$$\mathbb{E}[(X - \mathbb{E}[X])^2],$$
 (C2)

Skewness =
$$\frac{\mathbb{E}[(X - \mathbb{E}[X])^3]}{\mathbb{E}[(X - \mathbb{E}[X])^2]^{3/2}},$$
 (C3)

$$Kurtosis = \frac{\mathbb{E}[(X - \mathbb{E}[X])^4]}{\mathbb{E}[(X - \mathbb{E}[X])^2]^2},$$
 (C4)

and thus they can be estimated from the data. Furthermore, we used error propagation methods to estimate the standard statistical error on each of these quantities.

R. Islam, R. Ma, P. M. Preiss, M. Eric Tai, A. Lukin, M. Rispoli, and M. Greiner, Measuring entanglement entropy in a quantum many-body system, Nature 528, 77 (2015).

^[2] N. Laflorencie, Quantum entanglement in condensed matter systems, Physics Reports **646**, 1 (2016), quantum

entanglement in condensed matter systems.

^[3] R. Orús, Tensor networks for complex quantum systems, Nature Reviews Physics 1, 538 (2019).

^[4] E. Chitambar and G. Gour, Quantum resource theories, Rev. Mod. Phys. 91, 025001 (2019).

- [5] G. Carleo, I. Cirac, K. Cranmer, L. Daudet, M. Schuld, N. Tishby, L. Vogt-Maranto, and L. Zdeborová, Machine learning and the physical sciences, Rev. Mod. Phys. 91, 045002 (2019).
- [6] V. Dunjko and H. J. Briegel, Machine learning & artificial intelligence in the quantum domain: a review of recent progress, Reports on Progress in Physics 81, 074001 (2018).
- [7] D.-L. Deng, X. Li, and S. Das Sarma, Quantum entanglement in neural network states, Phys. Rev. X 7, 021021 (2017).
- [8] G. Carleo and M. Troyer, Solving the quantum manybody problem with artificial neural networks, Science 355, 602 (2017).
- [9] J. Carrasquilla, Machine Learning for Quantum Matter, arXiv: 2003.11040.
- [10] X. Guo, T. D. Barrett, Z. M. Wang, and A. I. Lvovsky, Backpropagation through nonlinear units for all-optical training of neural networks (2019), arXiv:1912.12256 [cs.ET].
- [11] W. Asavanant, Y. Shiozawa, S. Yokoyama, B. Charoen-sombutamon, H. Emura, R. N. Alexander, S. Takeda, J.-i. Yoshikawa, N. C. Menicucci, H. Yonezawa, and A. Furusawa, Generation of time-domain-multiplexed two-dimensional cluster state, Science 366, 373 (2019).
- [12] M. V. Larsen, X. Guo, C. R. Breum, J. S. Neergaard-Nielsen, and U. L. Andersen, Deterministic generation of a two-dimensional cluster state, Science 366, 369 (2019), https://science.sciencemag.org/content/366/6463/369.full.pdf.
- [13] M. Chen, N. C. Menicucci, and O. Pfister, Experimental realization of multipartite entanglement of 60 modes of a quantum optical frequency comb, Phys. Rev. Lett. 112, 120505 (2014).
- [14] Y.-S. Ra, A. Dufour, M. Walschaers, C. Jacquard, T. Michel, C. Fabre, and N. Treps, Non-gaussian quantum states of a multimode light field, Nature Physics 16, 144 (2020).
- [15] N. Biagi, L. S. Costanzo, M. Bellini, and A. Zavatta, Entangling macroscopic light states by delocalized photon addition, Phys. Rev. Lett. 124, 033604 (2020).
- [16] M. Walschaers, C. Fabre, V. Parigi, and N. Treps, Statistical signatures of multimode single-photon-added and -subtracted states of light, Phys. Rev. A 96, 053835 (2017).
- [17] Q. Zhuang, P. W. Shor, and J. H. Shapiro, Resource theory of non-gaussian operations, Phys. Rev. A 97, 052317 (2018).
- [18] F. Albarelli, M. G. Genoni, M. G. A. Paris, and A. Ferraro, Resource theory of quantum non-gaussianity and wigner negativity, Phys. Rev. A 98, 052350 (2018).
- [19] R. Takagi and Q. Zhuang, Convex resource theory of nongaussianity, Phys. Rev. A 97, 062337 (2018).
- [20] V. Cimini, M. Barbieri, N. Treps, M. Walschaers, and V. Parigi, Neural networks for detecting multimode wigner negativity, Phys. Rev. Lett. 125, 160504 (2020).
- [21] M. Walschaers, V. Parigi, and N. Treps, Practical framework for conditional non-gaussian quantum state preparation, PRX Quantum 1, 020305 (2020).
- [22] U. Chabaud, T. Douce, D. Markham, P. van Loock, E. Kashefi, and G. Ferrini, Continuous-variable sampling from photon-added or photon-subtracted squeezed states, Phys. Rev. A 96, 062307 (2017).
- [23] Y. Cai, J. Roslund, G. Ferrini, F. Arzani, X. Xu, C. Fabre, and N. Treps, Multimode entanglement in re-

- configurable graph states using optical frequency combs, Nat. Commun. 8, 15645 (2017).
- [24] J. Nokkala, F. Arzani, F. Galve, R. Zambrini, S. Maniscalco, J. Piilo, N. Treps, and V. Parigi, Reconfigurable optical implementation of quantum complex networks, New Journal of Physics 20, 053024 (2018).
- [25] F. Sansavini and V. Parigi, Continuous variables graph states shaped as complex networks: Optimization and manipulation, Entropy 22, 26 (2020).
- [26] F. Arzani, G. Ferrini, F. Grosshans, and D. Markham, Random coding for sharing bosonic quantum secrets, Phys. Rev. A 100, 022303 (2019).
- [27] M. E. J. Newman, Networks, second edition (Oxford University Press, 2018).
- [28] A. L. Barabási, Networks science (Cambridge University Press, 2016).
- [29] R. Albert and A.-L. Barabási, Statistical mechanics of complex networks, Rev. Mod. Phys. 74, 47 (2002).
- [30] S. N. Dorogovtsev, A. V. Goltsev, and J. F. F. Mendes, Critical phenomena in complex networks, Rev. Mod. Phys. 80, 1275 (2008).
- [31] G. Bianconi, Interdisciplinary and physics challenges of network theory, EPL (Europhysics Letters) 111, 56001 (2015).
- [32] A. Halu, S. Garnerone, A. Vezzani, and G. Bianconi, Phase transition of light on complex quantum networks, Phys. Rev. E 87, 022104 (2013).
- [33] L. Jahnke, J. W. Kantelhardt, R. Berkovits, and df. S. Havlin, Wave localization in complex networks with high clustering, Phys. Rev. Lett. 101, 175702 (2008).
- [34] R. Burioni, D. Cassi, M. Rasetti, P. Sodano, and A. Vezzani, Bose-einstein condensation on inhomogeneous complex networks, Journal of Physics B: Atomic, Molecular and Optical Physics 34, 4697 (2001).
- [35] O. Mülken and A. Blumen, Continuous-time quantum walks: Models for coherent transport on complex networks, Physics Reports 502, 37 (2011).
- [36] M. A. Valdez, D. Jaschke, D. L. Vargas, and L. D. Carr, Quantifying complexity in quantum phase transitions via mutual information complex networks, Phys. Rev. Lett. 119, 225301 (2017).
- [37] J. Nokkala, S. Maniscalco, and J. Piilo, Local probe for connectivity and coupling strength in quantum complex networks, Scientific Reports 8, 13010 (2018).
- [38] J. Biamonte, M. Faccin, and M. De Domenico, Complex networks from classical to quantum, Communications Physics 2, 53 (2019).
- [39] A. Cabot, F. Galve, V. M. Eguíluz, K. Klemm, S. Maniscalco, and R. Zambrini, Unveiling noiseless clusters in complex quantum networks, npj Quantum Information 4, 57 (2018).
- [40] S. Chakraborty, L. Novo, A. Ambainis, and Y. Omar, Spatial search by quantum walk is optimal for almost all graphs, Phys. Rev. Lett. 116, 100501 (2016).
- [41] M. Cuquet and J. Calsamiglia, Entanglement percolation in quantum complex networks, Phys. Rev. Lett. 103, 240503 (2009).
- [42] M. Faccin, P. Migdał, T. H. Johnson, V. Bergholm, and J. D. Biamonte, Community detection in quantum complex networks, Phys. Rev. X 4, 041012 (2014).
- [43] B. Sundar, M. A. Valdez, L. D. Carr, and K. R. Hazzard, Complex-network description of thermal quantum states in the ising spin chain, Physical Review A 97, 052320 (2018).

- [44] B. Buča, J. Tindall, and D. Jaksch, Non-stationary coherent quantum many-body dynamics through dissipation, Nature Communications 10, 1730 (2019).
- [45] B. Sokolov, M. A. C. Rossi, G. García-Pérez, and S. Maniscalco, Emergent entanglement structures and self-similarity in quantum spin chains (2020), arXiv:2007.06989 [quant-ph].
- [46] L. E. Hillberry, M. T. Jones, D. L. Vargas, P. Rall, N. Y. Halpern, N. Bao, S. Notarnicola, S. Montangero, and L. D. Carr, Entangled quantum cellular automata, physical complexity, and goldilocks rules (2020), arXiv:2005.01763 [quant-ph].
- [47] H. J. Kimble, The quantum internet, Nature 453, 1023 (2008).
- [48] A. M. Childs, Universal computation by quantum walk, Phys. Rev. Lett. **102**, 180501 (2009).
- [49] M. Mohseni, P. Rebentrost, S. Lloyd, and A. Aspuru-Guzik, Environment-assisted quantum walks in photosynthetic energy transfer, The Journal of Chemical Physics 129, 174106 (2008), https://doi.org/10.1063/1.3002335.
- [50] M. B. Plenio and S. F. Huelga, Dephasing-assisted transport: quantum networks and biomolecules, New Journal of Physics 10, 113019 (2008).
- [51] M. Walschaers, F. Schlawin, T. Wellens, and A. Buchleitner, Quantum transport on disordered and noisy networks: An interplay of structural complexity and uncertainty, Annual Review of Condensed Matter Physics 7, 223 (2016), https://doi.org/10.1146/annurev-conmatphys-031115-011327.
- [52] D. Awschalom, K. K. Berggren, H. Bernien, S. Bhave, L. D. Carr, P. Davids, S. E. Economou, D. Englund, A. Faraon, M. Fejer, S. Guha, M. V. Gustafsson, E. Hu, L. Jiang, J. Kim, B. Korzh, P. Kumar, P. G. Kwiat, M. Lončar, M. D. Lukin, D. A. B. Miller, C. Monroe, S. W. Nam, P. Narang, J. S. Orcutt, M. G. Raymer, A. H. Safavi-Naeini, M. Spiropulu, K. Srinivasan, S. Sun, J. Vučković, E. Waks, R. Walsworth, A. M. Weiner, and Z. Zhang, Development of quantum interconnects for next-generation information technologies (2019), arXiv:1912.06642 [quant-ph].
- [53] E. Altman, K. R. Brown, G. Carleo, L. D. Carr, E. Demler, C. Chin, B. DeMarco, S. E. Economou, M. A. Eriksson, K.-M. C. Fu, M. Greiner, K. R. Hazzard, R. G. Hulet, A. J. Kollár, B. L. Lev, M. D. Lukin, R. Ma, X. Mi, S. Misra, C. Monroe, K. Murch, Z. Nazario, K.-K. Ni, A. C. Potter, P. Roushan, M. Saffman, M. Schleier-Smith, I. Siddiqi, R. Simmonds, M. Singh, I. Spielman, K. Temme, D. S. Weiss, J. Vučković, V. Vuletić, J. Ye, and M. Zwierlein, Quantum simulators: Architectures and opportunities, PRX Quantum 2, 017003 (2021).
- [54] J. Roslund, R. Medeiros de Araújo, S. Jiang, C. Fabre, and N. Treps, Wavelength-multiplexed quantum networks with ultrafast frequency combs, Nat. Photon. 8, 109 (2014).
- [55] S. Yokoyama, R. Ukai, S. C. Armstrong, C. Sornphiphatphong, T. Kaji, S. Suzuki, J.-i. Yoshikawa, H. Yonezawa, N. C. Menicucci, and A. Furusawa, Ultra-large-scale continuous-variable cluster states multiplexed in the time domain, Nature Photonics 7, 982 (2013).
- [56] N. C. Menicucci, P. van Loock, M. Gu, C. Weedbrook, T. C. Ralph, and M. A. Nielsen, Universal quantum computation with continuous-variable cluster states, Phys. Rev. Lett. 97, 110501 (2006).

- [57] M. Gu, C. Weedbrook, N. C. Menicucci, T. C. Ralph, and P. van Loock, Quantum computing with continuousvariable clusters, Phys. Rev. A 79, 062318 (2009).
- [58] M. Walschaers, S. Sarkar, V. Parigi, and N. Treps, Tailoring non-gaussian continuous-variable graph states, Phys. Rev. Lett. 121, 220501 (2018).
- [59] Cluster is sometimes reserved for graphs allowing for universal quantum computing. In this work, however, we use the terms *cluster state* and *graph state* as synonyms.
- [60] R. Raussendorf and H. J. Briegel, A one-way quantum computer, Phys. Rev. Lett. 86, 5188 (2001).
- [61] R. Raussendorf, D. E. Browne, and H. J. Briegel, Measurement-based quantum computation on cluster states, Phys. Rev. A 68, 022312 (2003).
- [62] A. F. Verbeure, Bose systems, in Many-Body Boson Systems: Half a Century Later (Springer London, London, 2011) pp. 7–26.
- [63] C. Fabre and N. Treps, Modes and states in quantum optics, Rev. Mod. Phys. 92, 035005 (2020).
- [64] N. C. Menicucci, S. T. Flammia, and P. van Loock, Graphical calculus for gaussian pure states, Phys. Rev. A 83, 042335 (2011).
- [65] H. J. Briegel and R. Raussendorf, Persistent entanglement in arrays of interacting particles, Phys. Rev. Lett. 86, 910 (2001).
- [66] M. Van den Nest, A. Miyake, W. Dür, and H. J. Briegel, Universal resources for measurement-based quantum computation, Phys. Rev. Lett. 97, 150504 (2006).
- [67] M. Walschaers, C. Fabre, V. Parigi, and N. Treps, Entanglement and wigner function negativity of multimode non-gaussian states, Phys. Rev. Lett. 119, 183601 (2017).
- [68] M. Walschaers and N. Treps, Remote generation of wigner negativity through einstein-podolsky-rosen steering, Phys. Rev. Lett. 124, 150501 (2020).
- [69] Y.-S. Ra, C. Jacquard, A. Dufour, C. Fabre, and N. Treps, Tomography of a mode-tunable coherent singlephoton subtractor, Phys. Rev. X 7, 031012 (2017).
- [70] J. Wenger, R. Tualle-Brouri, and P. Grangier, Non-gaussian statistics from individual pulses of squeezed light, Phys. Rev. Lett. 92, 153601 (2004).
- [71] V. Parigi, A. Zavatta, M. Kim, and M. Bellini, Probing quantum commutation rules by addition and subtraction of single photons to/from a light field, Science 317, 1890 (2007).
- [72] A. Zavatta, S. Viciani, and M. Bellini, Quantum-toclassical transition with single-photon-added coherent states of light, Science 306, 660 (2004).
- [73] A. I. Lvovsky, P. Grangier, A. Ourjoumtsev, V. Parigi, M. Sasaki, and R. Tualle-Brouri, Production and applications of non-Gaussian quantum states of light, arXiv:2006.16985.
- [74] S. L. Zhang and P. van Loock, Distillation of mixed-state continuous-variable entanglement by photon subtraction, Phys. Rev. A 82, 062316 (2010).
- [75] S. Wang, L.-L. Hou, X.-F. Chen, and X.-F. Xu, Continuous-variable quantum teleportation with nongaussian entangled states generated via multiple-photon subtraction and addition, Phys. Rev. A 91, 063832 (2015).
- [76] X.-G. Meng, K.-C. Li, J.-S. Wang, X.-Y. Zhang, Z.-T. Zhang, Z.-S. Yang, and B.-L. Liang, Continuous-variable entanglement and wigner-function negativity via adding or subtracting photons, Annalen der Physik 532, 1900585 (2020).

- [77] R. W. Spekkens, Negativity and contextuality are equivalent notions of nonclassicality, Phys. Rev. Lett. 101, 020401 (2008).
- [78] A. Mari and J. Eisert, Positive wigner functions render classical simulation of quantum computation efficient, Phys. Rev. Lett. 109, 230503 (2012).
- [79] R. Takagi and Q. Zhuang, Convex resource theory of nongaussianity, Phys. Rev. A 97, 062337 (2018).
- [80] F. Arzani, N. Treps, and G. Ferrini, Polynomial approximation of non-gaussian unitaries by counting one photon at a time, Phys. Rev. A 95, 052352 (2017).
- [81] M. Yukawa, K. Miyata, H. Yonezawa, P. Marek, R. Filip, and A. Furusawa, Emulating quantum cubic nonlinearity, Phys. Rev. A 88, 053816 (2013).
- [82] C. K. Hong, Z. Y. Ou, and L. Mandel, Measurement of subpicosecond time intervals between two photons by interference, Phys. Rev. Lett. 59, 2044 (1987).
- [83] C. W. J. Beenakker, J. W. F. Venderbos, and M. P. van Exter, Two-photon speckle as a probe of multi-dimensional entanglement, Phys. Rev. Lett. 102, 193601 (2009).
- [84] M. Walschaers, Signatures of many-particle interference, Journal of Physics B: Atomic, Molecular and Optical Physics 53, 043001 (2020).
- [85] N. Somaschi, V. Giesz, L. De Santis, J. C. Loredo, M. P. Almeida, G. Hornecker, S. L. Portalupi, T. Grange, C. Antón, J. Demory, C. Gómez, I. Sagnes, N. D. Lanzillotti-Kimura, A. Lemaítre, A. Auffeves, A. G. White, L. Lanco, and P. Senellart, Near-optimal singlephoton sources in the solid state, Nature Photonics 10, 340 (2016).
- [86] L. c. v. Lachman, I. Straka, J. Hloušek, M. Ježek, and R. Filip, Faithful hierarchy of genuine n-photon quantum non-gaussian light, Phys. Rev. Lett. 123, 043601 (2019).
- [87] M. Walschaers, J. Kuipers, J.-D. Urbina, K. Mayer, M. C. Tichy, K. Richter, and A. Buchleitner, Statistical benchmark for BosonSampling, New Journal of Physics 18, 032001 (2016).
- [88] T. Giordani, F. Flamini, M. Pompili, N. Viggianiello, N. Spagnolo, A. Crespi, R. Osellame, N. Wiebe, M. Walschaers, A. Buchleitner, and F. Sciarrino, Exper-

- imental statistical signature of many-body quantum interference, Nature Photonics **12**, 173 (2018).
- [89] The case where $p_{\text{WS}} = 0.05$ forms an exception. Here we consider 74 realizations.
- [90] C. Navarrete-Benlloch, R. García-Patrón, J. H. Shapiro, and N. J. Cerf, Enhancing quantum entanglement by photon addition and subtraction, Phys. Rev. A 86, 012328 (2012).
- [91] C. S. Hamilton, R. Kruse, L. Sansoni, S. Barkhofen, C. Silberhorn, and I. Jex, Gaussian boson sampling, Phys. Rev. Lett. 119, 170501 (2017).
- [92] U. Chabaud, T. Douce, D. Markham, P. van Loock, E. Kashefi, and G. Ferrini, Continuous-variable sampling from photon-added or photon-subtracted squeezed states, Phys. Rev. A 96, 062307 (2017).
- [93] A. Deshpande, A. Mehta, T. Vincent, N. Quesada, M. Hinsche, M. Ioannou, L. Madsen, J. Lavoie, H. Qi, J. Eisert, D. Hangleiter, B. Fefferman, and I. Dhand, Quantum computational supremacy via high-dimensional gaussian boson sampling (2021), arXiv:2102.12474 [quant-ph].
- [94] H.-S. Zhong, H. Wang, Y.-H. Deng, M.-C. Chen, L.-C. Peng, Y.-H. Luo, J. Qin, D. Wu, X. Ding, Y. Hu, P. Hu, X.-Y. Yang, W.-J. Zhang, H. Li, Y. Li, X. Jiang, L. Gan, G. Yang, L. You, Z. Wang, L. Li, N.-L. Liu, C.-Y. Lu, and J.-W. Pan, Quantum computational advantage using photons, Science 370, 1460 (2020).
- [95] H.-S. Zhong, Y.-H. Deng, J. Qin, H. Wang, M.-C. Chen, L.-C. Peng, Y.-H. Luo, D. Wu, S.-Q. Gong, H. Su, Y. Hu, P. Hu, X.-Y. Yang, W.-J. Zhang, H. Li, Y. Li, X. Jiang, L. Gan, G. Yang, L. You, Z. Wang, L. Li, N.-L. Liu, J. Renema, C.-Y. Lu, and J.-W. Pan, Phaseprogrammable gaussian boson sampling using stimulated squeezed light (2021), arXiv:2106.15534 [quant-ph].
- [96] M. Walschaers, Code: Cv quantum complex networks (version 1) (2021).
- [97] D. S. Phillips, M. Walschaers, J. J. Renema, I. A. Walmsley, N. Treps, and J. Sperling, Benchmarking of gaussian boson sampling using two-point correlators, Phys. Rev. A 99, 023836 (2019).